article. A total of 100 copies of each protein fragment pair were equilibrated at 2000 K with the p53 side-chain atoms reduced in atomic radius, bond lengths, and electrostatic and van der Waals forces to create molecular models of the p53–CHC complex. The equilibrated molecules underwent simulated annealing along with growing the p53 side chains to their original sizes and energies. After generating a probability density map using the 100 copies of the p53–CHC complex, the best-fit structure was derived by simulated annealing to the probability density map of the complex. Resulting structural analyses by MCSA-PCR revealed that residues Leu43, Leu45, Ile50, and Trp53 of p53 were varied in the hydrophobic cavity of CHC and that Trp53 of p53 was stacked near Phe1327 of CHC through these aromatic rings (Fig. 3a). Notably, a side chain of Asn1288 of CHC appeared to contact a side chain of Gln38 of p53 (Fig. 3b); in contrast, Asn1288 of CHC is unlikely to be a contact site with CLC. In fact, a substitution of Asn1288 to Ala in CHC diminishes its ability to bind to p53 without any effect on CHC–CLC interaction, though CLC binds to a similar region in CHC with p53 (see below). Interestingly, this Asn1288 in CHC is a conserved residue in multicellular organisms from mammals to flies, but this residue is not present in unicellular organisms such as yeasts and fungi (Fig. 3c).

An Asn1288 residue in CHC is important for binding to p53

In order to examine the requirement of Asn1288 residue in CHC for binding to p53, we substituted Asn1288 to Ala of CHC bearing residues from 833 to 1406 to generate a CHC833–1406-N1288A mutant. The region from residues 833 to 1406 of CHC is defined as the interaction domain with p53 to trans-

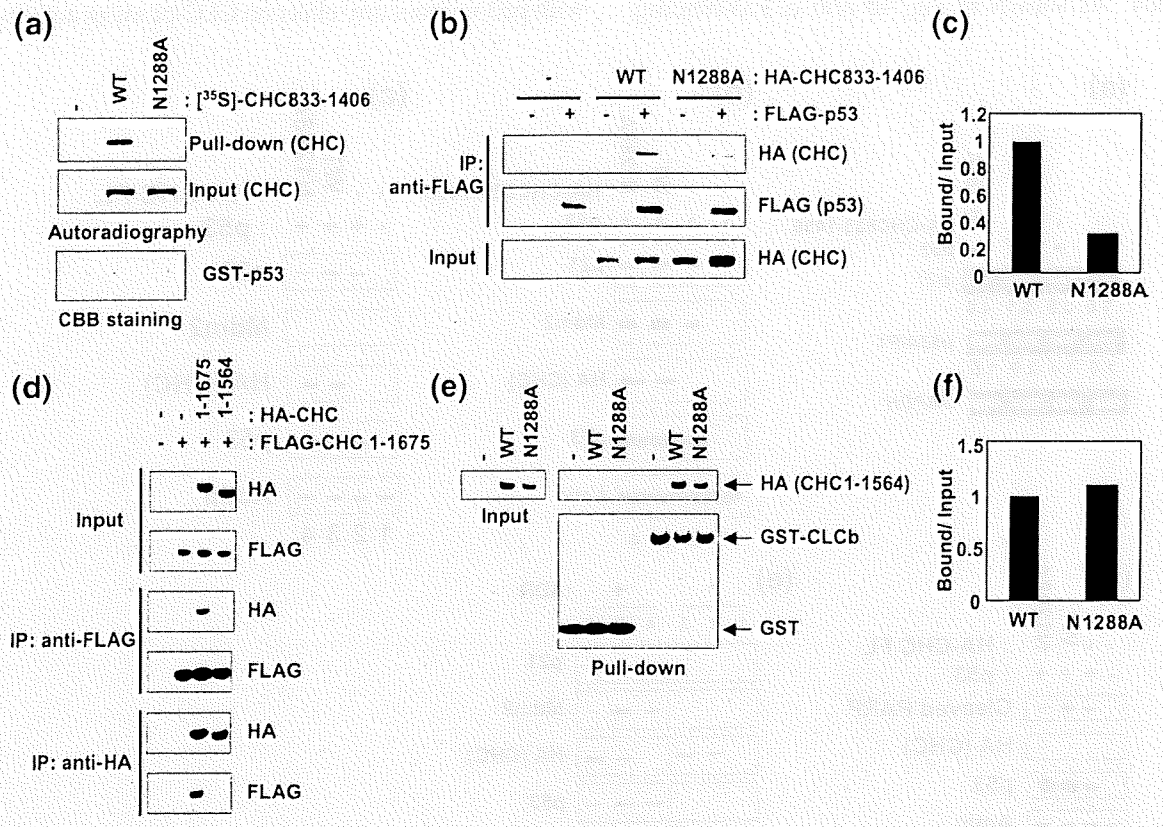

Fig. 4. Substitution of Asn1288 to Ala in CHC diminishes its ability to interact with p53. (a) *In vitro* binding assay for p53–CHC interaction. ^{35}S-labeled CHC833–1406 proteins (wild type and N1288A) were synthesized and used for *in vitro* binding assay as above. (b) Binding assay for p53–CHC interaction in cells. H1299 cells were transfected with FLAG-p53 and each HA-CHC833–1406 construct. FLAG-p53 was immunoprecipitated by anti-FLAG antibody, and eluates were loaded on a 5–20% gradient SDS-PAGE gel, followed by immunoblotting with anti-HA or anti-FLAG antibodies. (c) The graph represents the fold binding relative to input signal as quantified by Image J densitometry. (d) CHC lacking trimerization domain (CHC1–1564) does not interact with full-length CHC (CHC1–1675). H1299 cells were transfected with each HA-CHC construct and FLAG-CHC1–1675. Samples immunoprecipitated by either anti-HA or anti-FLAG antibody were separated by SDS-PAGE, followed by immunoblotting with indicated antibodies. The samples were run in the same gel and then combined side by side. (e) CHC1–1564 harboring N1288A interacts with CLC equivalent to wild-type CHC. HA-CHC1–1564 proteins (wild type and N1288A) were synthesized by an *in vitro* transcription-coupled translation system using rabbit reticulocyte lysates. Lysates containing HA-CHC protein were mixed with GST or GST-CLC immobilized on glutathione-Sepharose 4B beads for binding assay, separated by SDS-PAGE, and followed by immunoblotting with indicated antibodies. (f) The graph represents the fold binding relative to input signal as quantified by Image J densitometry.

activate it and has neither the ability to form trimerization nor the ability to bind to CLC.[21] The trimerization domain of CHC interacts with endogenous CHC, and the CLC-binding domain interferes with the binding of p53 to CHC.[21] Thus, these domains may be obstructed to assess the effect of a point mutation of CHC on the interaction with p53 and we used a CHC deletion mutant lacking trimerization and CLC-binding domains for an *in vitro* p53-binding assay. A GST pull-down assay showed that an N1288A mutation in the CHC833–1406 protein diminished its ability to interact with p53, although wild-type CHC was able to bind p53 (Fig. 4a). Furthermore, we tested whether N1288A of CHC causes decreased p53-binding affinity in cells. A FLAG-tagged p53 construct was cotransfected with empty vector, HA-tagged CHC833–1406-WT, or HA-tagged CHC-833–1406-N1288A in cells, and cell lysates were immunoprecipitated with anti-FLAG antibody followed by immunoblotting with anti-HA antibody. As shown in Fig. 4b and c, p53-binding affinity of mutated CHC was reduced up to 30% compared with wild-type CHC, indicating that this N1288 residue in CHC protein is crucial for interaction between CHC and p53. We have previously found that CLC binds to CHC at the C-terminal region proximal to p53-binding sites and inhibits the interaction of p53 with CHC. To assess whether this substitution affects CLC-binding activity, we constructed an N1288A mutant of CHC lacking residues from 1565 to 1675 (CHC1–1564), which does not possess a trimerization domain that interacts with full-length CHC (Fig. 4d), and performed a GST pull-down assay using GST fused to CLCb (GST-CLCb). HA-tagged CHC1–1564 proteins produced by an *in vitro* transcription/translation system using rabbit reticulocyte lysates were used for this assay. Interestingly, the N1288A mutation had little effect on the ability to interact with CLC (Fig. 4e and f). Taken together, these results indicate that an N1288A mutation of CHC specifically influences interaction with p53 without any effect on CLC-binding activity.

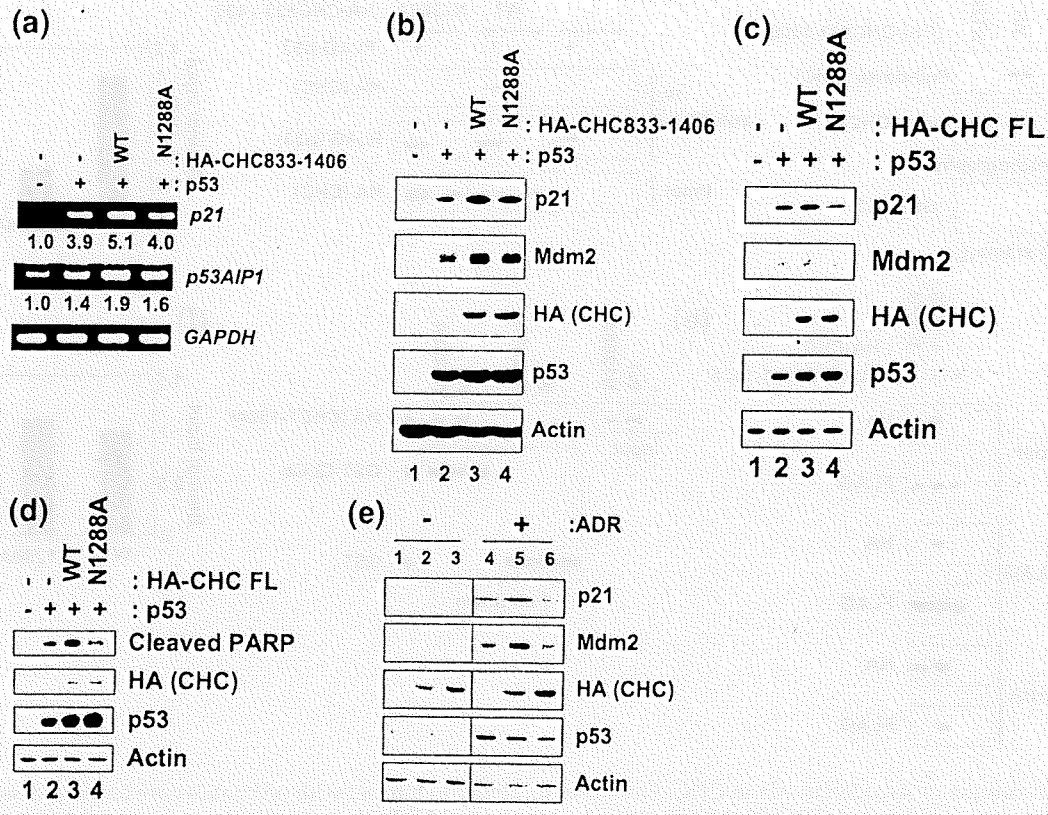

Fig. 5. An N1288A mutation of CHC abolishes the ability to transactivate p53. (a) H1299 cells were transfected with p53 and each HA-CHC833–1406 construct. Expression levels of p53-target genes were analyzed by semiquantitative RT-PCR. The intensity of PCR products was quantified by Image J software. (b) H1299 cells were transfected as described in (a), and whole-cell lysates were analyzed by immunoblotting using the indicated antibodies. (c) Full-length CHC-N1288A acts as a dominant-negative mutant. H1299 cells were transfected with p53 and each HA-tagged full-length CHC construct, and whole-cell lysates were analyzed by immunoblotting using the indicated antibodies. (d) Full-length CHC-N1288A inhibits p53-mediated apoptosis. H1299 cells were transfected with p53 and each HA-tagged CHC construct, incubated for 24 h, and the cleaved PARP was detected by immunoblotting with anti-cleaved PARP antibody. (e) Full-length CHC-N1288A blocks the induction of p53-target genes activated by DNA damage. HT-1080 cells were transfected with an empty vector, wild-type CHC, or CHC-FL-N1288A construct, and stable transformants were obtained by G418 selection. These cells were treated without (lanes 1 to 3) or with (lanes 3 to 6) 0.5 μM adriamycin (ADR) for 6 h. Cell lysates from cells transfected with empty vector (lanes 1 and 4), wild-type CHC (lanes 2 and 5), or CHC-FL-N1288A (lanes 3 and 6) were subjected to immunoblotting with indicated antibodies.

CHC-N1288A mutant abolishes the ability to transactivate p53

Given that the N1288 residue in CHC is crucial for interaction with p53, we next examined the effect of an N1288A mutation of CHC on p53 transactivation. Reverse transcriptase–polymerase chain reaction (RT-PCR) analysis revealed that CHC833–1406-WT had the activity to enhance p53 transactivation, but CHC833–1406-N1288A failed to enhance the induction of p53-target genes such as p21 and p53AIP1 (Fig. 5a). In addition, we confirmed that CHC833–1406-N1288A abolished the ability to enhance the induction of p53-target genes by immunoblot analysis (Fig. 5b). To further confirm the effect of N1288A mutation on p53-mediated transcription, we used full-length CHC constructs with or without this mutation. Full-length wild-type CHC increased expression levels of both p21 and Mdm2 in a p53-dependent manner; in contrast, full-length CHC harboring an N1288A mutation (CHC-FL-N1288A) abrogated the ability to enhance p53 transactivation (Fig. 5c). Interestingly, CHC-FL-N1288A appears to behave as a dominant-negative mutant.

Expression of p53 in p53-null cells induces apoptosis accompanied with caspase-3/7 activation and the cleavage of poly-ADP ribose polymerase (PARP) known as a substrate of caspase-3/7.[13,21]

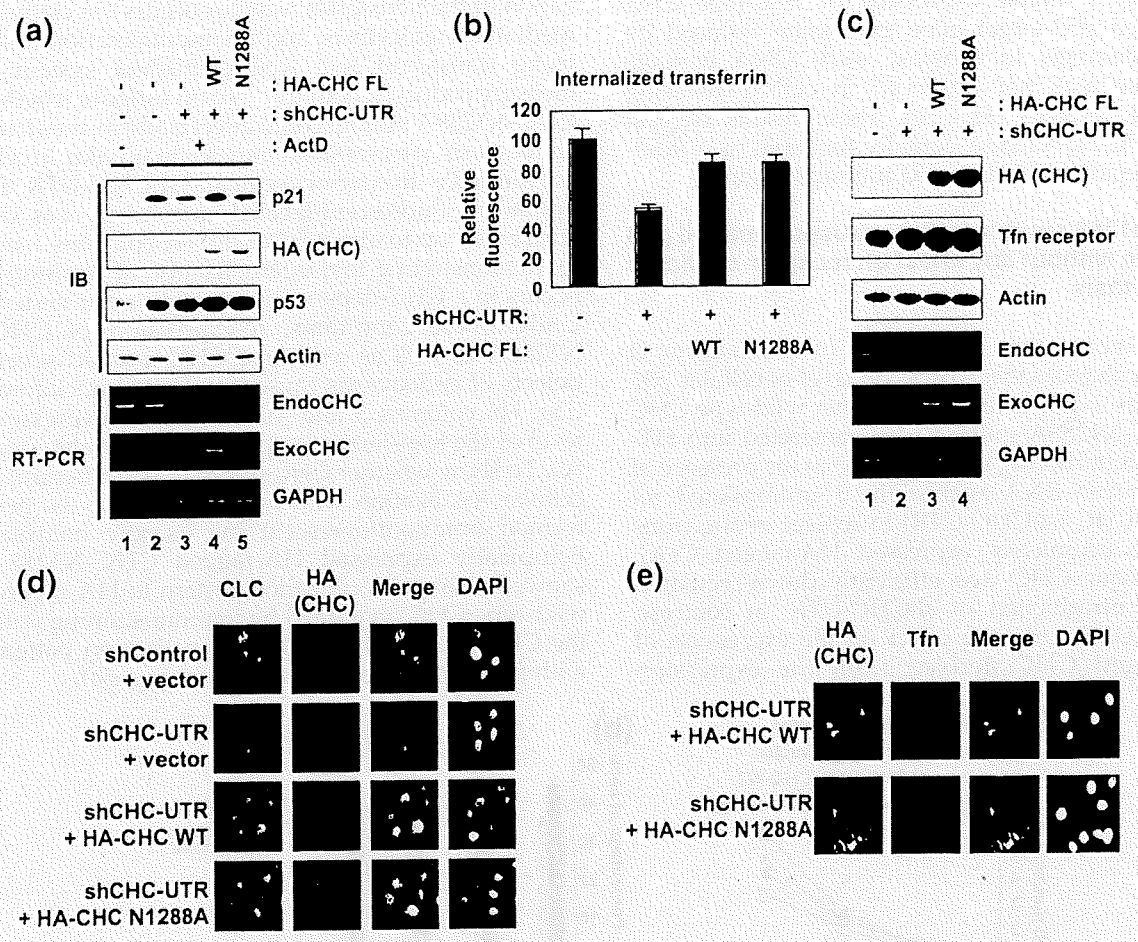

Fig. 6. An N1288A mutation in full-length CHC causes a severe defect in the regulation of p53-mediated transcription, but its CHC mutant preserves function for receptor-mediated endocytosis. (a) HT-1080 cells were transfected with shCHC-UTR and each HA-tagged full-length CHC construct, treated with 5 nM ActD for 6 h, and cell lysates were analyzed by immunoblotting using the indicated antibodies and by RT-PCR using primers specific for endogenous CHC (EndoCHC) and ectopically expressed CHC (ExoCHC). Actin and GAPDH were used as loading controls for immunoblotting and RT-PCR, respectively. (b) HeLa cells were transfected with indicated plasmids plus a green fluorescent protein expression plasmid. Three days after transfection, cells were incubated for 8 min at 37 °C in DMEM containing 20 μg/mL of AlexaFluor594-conjugated transferrin (AF594-transferrin) and 0.1% BSA. After the removal of cell-surface-bound AF594-transferrin, these cells were trypsinized and fixed with 4% paraformaldehyde. For measurement of AF594-transferrin uptake, green fluorescent protein-positive cells were quantified by flow cytometric analysis. (c) Proteins and total RNA in whole-cell lysates from cells used for (b) were analyzed by immunoblotting and RT-PCR, respectively. (d) A CHC-N1288A mutant co-localizes with CLC, similarly to wild-type CHC. HeLa cells were transfected with the indicated plasmids and immunostained with anti-HA (green) and anti-CLC (red) antibodies 72 h after transfection. (e) An N1288A mutation has little effect on the localization of transferrin. HeLa cells were transfected with the indicated plasmids, and the uptake of AF594-transferrin (red) was carried out as in (b). After the removal of cell-surface-bound AF594-transferrin, these cells were immunostained with anti-HA (green) antibody.

Therefore, we next addressed the effect of an N1288A mutation in full-length CHC on p53-mediated apoptosis. Caspase activation is an important event for apoptosis and it was monitored using the cleavage of PARP. Immunoblot analysis showed that co-expression of p53 and wild-type CHC increased cleavage of PARP compared with p53 alone (Fig. 5d), consistent with our previous data that CHC enhances p53-mediated apoptosis. In contrast, CHC-N1288A inhibited p53-induced PARP cleavage (Fig. 5d), suggesting that an N1288A mutation in CHC abolishes the ability to undergo apoptosis mediated by p53. To evaluate CHC-FL-N1288A works as a dominant-negative effect, we generated cells stably expressing CHC-FL-N1288A. Stable expression of wild-type CHC enhanced p53-target gene expression induced by DNA damage; in contrast, such DNA damage response was not observed in cells expressing CHC-FL-N1288A (Fig. 5e). These results suggest that CHC-FL-N1288A actually functions as a dominant-negative effect on p53 transactivation.

An Asn1288 residue in CHC causes impaired p53 function without any effect on receptor-mediated endocytosis

It is known that a low dose of actinomycin D (ActD) enhances the expression level of cellular p53 and leads to p53 activation.[27] Either wild-type CHC or CHC-N1288A mutant was transfected into HT-1080 cells harboring wild-type p53 in the presence of short-hairpin RNA against the 3′-untranslated region of CHC (shCHC-UTR) to replace endogenous CHC to ectopically expressed HA-tagged CHC. Endogenous CHC was efficiently down-regulated by the introduction of shCHC-UTR; in contrast, shCHC-UTR had little effect on the expression of HA-tagged CHC derived from the expression plasmid, as confirmed by RT-PCR using primers specific for endogenous and ectopically expressed CHC (Fig. 6a). Partial knockdown of CHC attenuates the induction of p21 in response to ActD (Fig. 6a, lanes 2 and 3), as shown in our previous report.[5] Re-expression of HA-tagged wild-type CHC in CHC-depleted cells recovered DNA damage response to up-regulate p21 expression (Fig. 6a, lanes 3 and 4), whereas swapping of endogenous CHC with HA-tagged CHC bearing a N1288A mutation did not rescue p21 induction (Fig. 6a, lane 5). Taken together, these results demonstrate that Asn1288 in CHC is crucial for interaction with p53 to promote sufficient induction of p53-mediated transcription.

It has been shown that ligand-induced internalization of the transferrin receptor occurs via clathrin-mediated endocytosis, and an internalization assay using transferrin is a well-established system to measure endocytic activity.[28] To investigate whether CHC-N1288A mutant could affect clathrin-mediated endocytosis, we examined transferrin uptake. In cells transfected with control vector and shCHC-UTR, the uptake of fluorescent-labeled transferrin was decreased by up to about 50% (Fig. 6b, columns 1 and 2), demonstrating that internalization of transferrin occurs in a CHC-dependent manner in our system. Under these conditions, re-expression of CHC-N1288A as well as wild-type CHC rescued severe defects of endocytosis caused by CHC knockdown (Fig. 6b, columns 3 and 4), though the expression level of the transferrin receptor was invariable (Fig. 6c). To show whether CHC-N1288A exhibits similar cellular localization with wild-type CHC, we performed immunofluorescent microscopic analysis. Ectopically expressed HA-tagged CHC-N1288A showed a similar localization pattern to HA-tagged wild-type CHC, as judged by immunostaining with the CLC (Fig. 6d) or by the co-localization pattern with fluorescent-labeled transferrin (Fig. 6e).

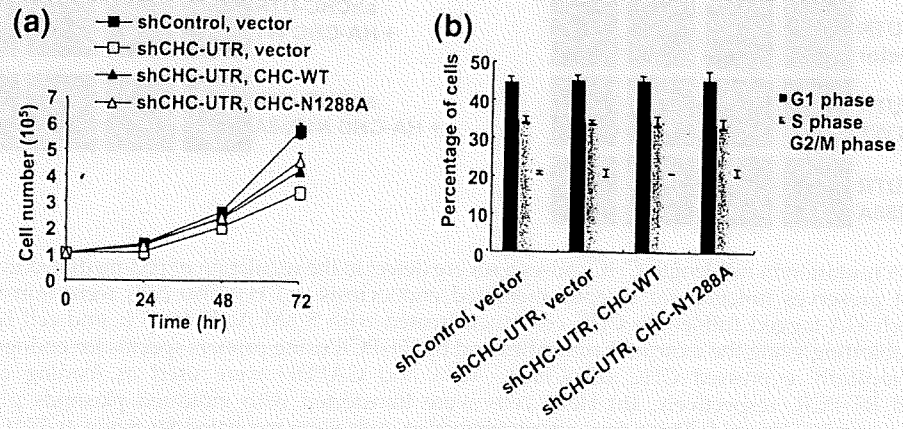

Fig. 7. An N1288A mutation in CHC has little or no effect on cell viability and cell-cycle progression. (a) A CHC-N1288A mutant has the ability to recover the proliferation of CHC-depleted cells as efficiently as that of wild-type CHC. Twenty-four hours after transfection with the indicated plasmids, these HT-1080 cells were collected and then plated in 60-mm culture dishes. Cell numbers were determined with a hemocytometer after the indicated times. Data represent the mean values from three independent experiments with error bars. (b) N1288A mutation did not impact on cell-cycle progression. HT-1080 cells were transfected as in (a), and these cells cultured for 72 h after transfection were subjected to flow cytometric analysis. DNA content was monitored by propidium iodide staining, and the percentages of the cells in G1, S, and G2/M phases were determined using ModFit LT software. Data represent the mean values from three independent experiments with error bars.

CHC is an essential gene for cell viability, and complete ablation of CHC expression leads to cell death.[20] Therefore, we next assessed whether an N1288A mutation in CHC influences cell viability. As shown in Fig. 7a, CHC-depleted cells expressing CHC-FL-N1288A exhibited no lethality, unlike CHC-depleted cells transfected with a control vector, and they showed a similar growth rate to CHC-depleted cells re-expressing wild-type CHC. We also confirmed that N1288A mutation did not influence mitosis as judged by flow cytometric analyses (Fig. 7b). Taken together, these data demonstrate that an N1288A mutation in CHC abolishes its abilities to interact with and to transactivate p53 without any effects on receptor-mediated endocytic activity and cell viability. Our findings provide a useful tool for understanding a role of CHC in p53-mediated transcription, distinct from receptor-mediated endocytosis.

Discussion

CHC has originally been identified as a cytosolic protein that functions in vesicle transport and endocytosis.[10–12] It has recently been shown that CHC is also involved in the maintenance of mitotic spindle as its additional function.[19] We have previously found an alternative function of CHC that promotes p53-mediated transcription in nuclei and that the enhancement of p53 transactivation by CHC required the interaction of the N-terminal transactivation domain of p53 with CHC.[13] Although the trimerization domain of CHC is important for functions in vesicle transport, endocytosis, and mitosis,[23] it is indispensable for p53-mediated transcription. These findings implicate that nuclear CHC works via a distinct mechanism from cytosolic CHC.[21] In addition, our recent studies showed that partial knockdown of CHC attenuated p53 transactivation, but we could not rule out a possibility that CHC knockdown may cause undetectable side effects on CHC-mediated endocytosis essential for cell survival and proliferation.[20]

We have previously noticed that the N-terminal region of p53 around Ser46 has a considerable similarity with the CHC-binding region of CLC and an essential Trp residue for binding to CHC in CLC is conserved in p53.[13] Conceivably, CLC competes with p53 through this homologous region in binding to CHC, and both p53 and CLC associate with CHC in a mutually exclusive manner.[13] In this study, we generated various p53 point mutants and determined the detailed residues responsible for binding to CHC. *In vitro* binding assay revealed that several hydrophobic residues, including Trp53 in p53, are required for interaction with CHC. Furthermore, mutations of these hydrophobic residues in p53 strikingly impaired the transcriptional activity compared with wild-type p53. Thus, these results indicate that conserved residues between p53 and CLC are required for both CHC binding and p53 transactivation and that the ability of p53 to interact with CHC correlates with p53 transcriptional activity.

We generated more than 20 constructs for CHC fragments containing the p53-binding region to determine the tertiary structure of the p53–CHC complex, but these CHC fragments had poor solubility and it was difficult to obtain the structural information of the p53–CHC complex (data not shown). Therefore, based on tertiary structures of the N-terminus of p53 and CHC already determined by NMR and X-ray crystallography in combination with information obtained from our present p53–CHC-binding studies, a preliminary molecular model of the p53–CHC interaction was constructed, although it remains to be determined whether CHC induces α-helical conformation of the N-terminus of p53, which is observed when forming a complex with RPA70 (replication protein A70) or with p62, a subunit of TFIIH.[24,25] This molecular modeling predicted that Asn1288 in CHC might be important for p53–CHC interaction because this residue is close to a side chain of Glu38 of p53. As expected, a substitution of the Asn1288 to Ala diminished the ability to bind p53 and to enhance p53 transactivation. We also found that an Asn-to-Ala-substituted full-length CHC (CHC-FL-N1288A) appears to behave as a dominant-negative mutant unlike CHC833–1406-N1288A. These findings suggest that the region depleted in CHC competes with endogenous CHC to trap some p53 co-activators, such as p300/CBP, because CHC interacts with p300/CBP to stabilize the association with p53.[13] On the other hand, CHC-FL-N1288A did not affect the ability to bind to CLC, transferrin uptake, and the cellular localization of CLC, and growth arrest induced by endogenous CHC knockdown was reverted by the expression of CHC-FL-N1288A as well as the introduction of wild-type CHC. In respect to the impact of partial CHC knockdown on G2/M phase, no alteration was observed, at least under our conditions. Taken together, these results suggest that this mutant influences the p53 pathway without any effect on CHC-mediated endocytosis essential for cell survival.

CHC is an essential gene for cell viability, and complete ablation of CHC expression leads to cell death accompanied by the activation of Akt-mediated and mitogen-activated protein kinase-mediated pathways.[20] In contrast, point mutations of some essential genes have often little effect on cell viability. For example, cytochrome *c* plays important roles in electron transport and apoptosis, but cytochrome *c* bearing a K72A point mutation is defective in apoptotic regulation without affecting the function of electron transport essential for cell viability.[31] Therefore, such a CHC point mutant will help to dissect physiological functions of CHC in the regulation of the p53 pathway.

Interestingly, the alignment of primary structures between species revealed that this Asn1288 in CHC was conserved in multicellular organisms from mammals to flies, but this amino acid residue was not present in unicellular organisms such as yeasts

and fungi (Fig. 2c). In multicellular organisms, the p53–CHC system may have evolved to acquire a complicated regulatory function in response to various cellular damages to maintain multicellular homeostasis.

In summary, we predicted a preliminary binding interface between p53 and CHC and found that an Asn1288 in CHC was critical for interaction with p53 but not with CLC. Using such a CHC mutant preserving endocytic function, specific disruption of the function of CHC as a p53 regulator in mice will clarify physiological functions of CHC in the regulation of the p53 pathway. In addition, there are no reports of cancer-associated mutations in the CHC gene so far and it is interesting to search for mutations in the p53-binding region of CHC, in particular the region around Asn1288, in tumor samples from patients. Further investigations will be needed to elucidate the role of CHC in tumorigenesis.

Materials and Methods

Cell culture and transfection

Human lung carcinoma H1299 cells were grown in RPMI 1640 medium supplemented with 10% fetal bovine serum and penicillin/streptomycin. Human fibrosarcoma HT-1080 cells and human cervical carcinoma HeLa cells were grown in Dulbecco's modified Eagle's medium (DMEM) supplemented with 10% fetal bovine serum and penicillin/streptomycin at 37 °C in a 5% CO_2 atmosphere. For transfection, cells were plated at 80–90% confluency the day before transfection and transfected with Lipofectamine 2000 reagent (Invitrogen) according to the manufacturer's protocol.

Antibodies

Horseradish peroxidase (HRP)-conjugated anti-p53 (DO-1), HRP-conjugated anti-Actin (C-2), anti-CLC (CON.1), and anti-GST (B-14) antibodies were purchased from Santa Cruz Biotechnology Inc. Anti-p21 (SX118) and anti-CHC (clone 23) antibodies were from BD Pharmingen. Anti-HA (6E2), anti-HA (C29F4), and anti-cleaved PARP antibodies were obtained from Cell Signaling Technology. Anti-Mdm2 (IF2), anti-FLAG (M2), and anti-transferrin receptor antibodies were purchased from Calbiochem, SIGMA, and Zymed, respectively. HRP-conjugated secondary antibodies were obtained from GE Healthcare.

Immunoprecipitation and immunoblot analysis

H1299 cells were extracted with lysis buffer [50 mM Tris at pH 7.2, 250 mM NaCl, 2 mM $MgCl_2$, 0.1 mM ethylenediaminetetraacetic acid, 0.1 mM ethylene glycol bis(β-aminoethyl ether)*N*,*N*′-tetraacetic acid, 0.1% Nonidet P-40, 0.5 mM DTT, 10 μg/mL antipain, 10 μg/mL pepstatin A, 10 μg/mL chymostatin, 10 μg/mL leupeptin, 10 μg/mL E-64, 10 μg/mL PMSF, 1 mM Na_3VO_4, and 5 mM NaF] for 20 min on ice, and the lysates were cleared by centrifugation at 20,000*g* for 20 min. For immunoprecipitation, the supernatants were incubated with 10 μL of anti-FLAG M2 agarose beads (SIGMA) for 3 h at 4 °C and washed three times with lysis buffer. The bound proteins were eluted with FLAG peptide (SIGMA) at 4 °C for 30 min, separated by SDS-PAGE (Biocraft), followed by transfer to polyvinylidene fluoride membranes (Millipore). The membranes were blocked with 5% skim milk in TBST buffer (20 mM Tris at pH 7.6, 137 mM NaCl, and 0.1% Tween 20) and incubated with the first antibody. The blots were washed three times with TBST buffer, incubated with the secondary antibody conjugated to HRP, and then washed five times with TBST buffer. The bands of interest were visualized by ECL chemiluminescence (GE Healthcare).

Reporter assay

A reporter assay was performed as described previously.[13] In brief, H1299 cells plated on 24-well plates were transfected with 1 ng of p53-SN3 and 150 ng of the indicated reporter vectors in combination with 10 ng of phRG-TK encoding Renilla luciferase as an internal control using Lipofectamine 2000. Twenty-four hours after transfection, cells were harvested and luciferase activity was quantified by a dual luciferase assay system (Promega) according to the manufacturer's instructions.

RT-PCR analysis

RT-PCR analysis was performed as described previously.[13] Briefly, total RNA was isolated using an RNeasy Mini kit (QIAGEN) and reverse-transcribed with the SuperScript First-Strand Synthesis System for RT-PCR kit (Invitrogen). Reverse-transcribed products were used in the PCR reactions. PCR programs and primer sequences were described previously.[13] PCR products were analyzed using 2% agarose gel electrophoresis and ethidium bromide staining. The amplified DNA fragments were quantified by Image J version 1.41 densitometry.

GST pull-down assay

To analyze the interaction between p53 and CHC, we performed a GST pull-down assay as described previously.[13] In brief, bacterial lysates containing p53 derivatives fused to GST were incubated with glutathione-Sepharose 4B beads (GE Healthcare) and washed extensively with binding buffer [50 mM Tris at pH 7.2, 250 mM NaCl, 2 mM $MgCl_2$, 0.1 mM ethylenediaminetetraacetic acid, 0.1 mM ethylene glycol bis(β-aminoethyl ether)*N*,*N*′-tetraacetic acid, 0.1% Tween 20, 0.5 mM DTT, 10 μg/mL antipain, 10 μg/mL pepstatin A, 10 μg/mL chymostatin, 10 μg/mL leupeptin, 10 μg/mL E-64, 10 μg/mL PMSF, 1 mM Na_3VO_4, and 5 mM NaF]. ^{35}S-labeled CHC derivatives were synthesized using an *in vitro* transcription/translation-coupled reticulocyte lysate system (Promega) and incubated with the above beads immobilized with GST-p53 derivatives at 4 °C for 2 h. After washing with 1 mL of binding buffer, bound proteins were eluted by boiling in SDS sample buffer for 5 min, subjected to SDS-PAGE, and analyzed by autoradiography.

RNA interference

For the expression of short-hairpin RNA against the 3′-UTR of CHC mRNA, synthetic oligo DNAs, 5′-GATCCCCAGAGCACCATGATTCCAATTTCAAGAGATTGGAATCATGGTGCTCTTTTTTGGAAA-3′ and 5′-

AGCTTTTCCAAAAAGAGCACCATGATTC-CAATTCTCTTGAAATTGGAATCATGGTGCTCTGGG-3′, were annealed and inserted into the pSUPER vector (shCHC-UTR) and transfected in HT-1080 and HeLa cells, as described above. To confirm the suppression of endogenous CHC expression, we used synthetic primers: CHC-S (5′-CCAGGCACCTTTTGGTTATG-3′) and CHC-AS (5′-CTTTCATGCCTCCCTAATGC-3′) for the detection of endogenous CHC and CHC-S and pcDNA3.1-AS (5′-ACTCAGACAATGCGATGCAA-3′) or pCAGGS-AS (5′-CCCATATGTCCTTCCGAGTG-3′) for ectopically expressed CHC.

Endocytosis assay, cell proliferation, and cell-cycle analyses

To analyze the effect of CHC mutants on endocytic activity, we transfected HeLa cells with 1 μg of shCHC-UTR plus 2 μg of pCAGGS-CHC vectors in combination with 50 ng of pmaxGFP vector (Amaxa), as a transfection marker. Three days after transfection, cells were incubated in DMEM containing 0.1% bovine serum albumin (BSA) for 3 h, followed by treatment with 20 μg/mL Alexafluor594-conjugated transferrin (AF594-transferrin, Molecular Probes) for 8 min at 37 °C. Cells were rapidly chilled by extensive washing with ice-cold PBS, and then AF594-transferrin bound on the cell surface was removed by washing with ice-cold acid-washing buffer containing 0.2 M acetic acid (pH 4.5) and 0.5 M NaCl. These cells were trypsinized, fixed with 4% paraformaldehyde in PBS for 20 min at room temperature, and resuspended in 0.1% BSA in PBS. Relative fluorescence was quantified by flow cytometric analysis (Becton Dickinson) for internalized AF594-transferrin.

HT-1080 cells transfected with the indicated expression vectors were collected 24 h after transfection and then plated in 60-mm culture dishes to analyze the effect of CHC-N1288A on cell proliferation. Cell numbers were determined with a hemocytometer after the indicated times.

For cell-cycle analysis, HT-1080 cells were transfected with the indicated expression vectors for 72 h and then fixed in 70% ethanol at −20 °C for several hours. Cells were centrifuged at 600*g* for 5 min and resuspended in PBS containing 0.1 mg/mL RNase A (QIAGEN). Samples were incubated at 37 °C for 30 min, and propidium iodide (SIGMA) was added to make a final concentration of 25 μg/mL. Samples were analyzed by a FACSCalibur flow cytometer using CellQuest software (BD Biosciences), and the percentages of the cells in G1, S, and G2/M phases of the cell cycle were determined using ModFit LT software.

Immunofluorescence

HeLa cells transfected with shCHC-UTR and pCAGGS-CHC were plated on an 8-well Lab-Tek II Chamber Slide (Nalge Nunc), fixed in 4% paraformaldehyde in PBS for 20 min, permeabilized with 0.1% Triton X-100 in PBS for 5 min, and blocked with PBS containing 3% BSA. The cells were sequentially incubated with anti-HA (C29F4) and/or anti-CLC antibodies and with AlexaFluor-conjugated secondary antibody (Molecular Probes) and mounted with a Vectashield reagent with 4′,6-diamidino-2-phenylindole (Vector Laboratories). Immunofluorescence was performed using a Nikon ECLIPSE E1000 fluorescence microscope (Nikon Corporation).

Structural modeling of p53–CHC interaction

To generate an initial model of the side chains in the p53–CHC interface, we used a model of CLC and CHC interface[23] as a template. A partial structure of p53 (residues 33–56) taken from the crystallographic structure of p53/RPA70 complex[24] was then overlaid manually to the backbone atoms of the corresponding region of CLC. The detailed backbone orientation was further established by rotational search and energy minimization. This docked model served as the starting point for MCSA-PCR. During the MCSA-PCR, all side-chain atoms of p53 were free to move, and backbone C^{α} atoms in the second α-helix of p53 (residue 46–56) were weakly restrained (5 kcal mol^{-1} $Å^{-2}$) to the corresponding residues of CLC (residue 97–107). For the first α-helix of p53 (residue 35–40), nuclear Overhauser effect distance restraints (2.86± 1 Å) were weakly assigned between the p53 backbone carbonyls and amides in order to promote the helicity of p53, but allowing the deviation from the original helix structure. Then, an ensemble of 100 possible structures was produced by growing side-chain atoms with simulated annealing methods. This was refined to a single best-fit structure through MCSA-pseudo-crystallographic refinement.[24] The final structure was refined against a pseudo-density map generated from the ensemble using standard crystallographic techniques. All calculations were carried out in gas phase with X-PLOR, using the OPLS (optimized potentials for liquid simulations) force field for polar hydrogens.[25]

Acknowledgements

We thank B. Vogelstein for WWP-Luc and the members of Taya and Yokota lab for helpful discussions. This work was partly supported by SORST, Japan Science and Technology Corporation (to Y.T.), MEXT, KAKENHI (17013088) (to Y.T. and M.E.), a Grant-in-Aid from the Ministry of Health, Labor and Welfare for the 3rd Term Comprehensive 10-year Strategy for Cancer Control (to Y.T. and M. E.), and a grant from the Takeda Science Foundation (to M.E.).

References

1. Toledo, F. & Wahl, G. M. (2006). Regulating the p53 pathway: in vitro hypotheses, in vivo veritas. *Nat. Rev. Cancer*, **6**, 909–923.
2. Bourdon, J. C., Laurenzi, V. D., Melino, G. & Lane, D. (2003). p53: 25 years of research and more questions to answer. *Cell Death Differ.* **10**, 397–399.
3. Vousden, K. H. & Lu, X. (2002). Live or let die: the cell's response to p53. *Nat. Rev. Cancer*, **2**, 594–604.
4. Vogelstein, B., Lane, D. & Levine, A. J. (2000). Surfing the p53 network. *Nature*, **408**, 307–310.
5. Ljungman, M. (2000). Dial 9-1-1 for p53: mechanisms of p53 activation by cellular stress. *Neoplasia*, **2**, 208–225.
6. Prives, C. & Hall, P. A. (1999). The p53 pathway. *J. Pathol.* **187**, 112–126.
7. Levine, A. J. (1997). p53, the cellular gatekeeper for growth and division. *Cell*, **88**, 323–331.

8. Hollstein, M., Sidransky, D., Vogelstein, B. & Harris, C. C. (1991). p53 mutations in human cancers. *Science*, **253**, 49–53.
9. Samuels-Lev, Y., O'Connor, D. J., Bergamaschi, D., Trigiante, G., Hsieh, J. K., Zhong, S. *et al.* (2001). ASPP proteins specifically stimulate the apoptotic function of p53. *Mol. Cell*, **8**, 781–794.
10. Willingham, M. C. & Pastan, I. (1984). Endocytosis and exocytosis: current concepts of vesicle traffic in animal cells. *Int. Rev. Cytol.* **92**, 51–92.
11. Takei, K. & Haucke, V. (2001). Clathrin-mediated endocytosis: membrane factors pull the trigger. *Trends Cell Biol.* **11**, 385–391.
12. Mellman, I. (1996). Endocytosis and molecular sorting. *Annu. Rev. Cell Dev. Biol.* **12**, 575–625.
13. Enari, M., Ohmori, K., Kitabayashi, I. & Taya, Y. (2006). Requirement of clathrin heavy chain for p53-mediated transcription. *Genes Dev.* **20**, 1087–1099.
14. Ishii, K., Hirano, Y., Araki, N., Oda, T., Kumeta, M., Takeyasu, K. *et al.* (2008). Nuclear matrix contains novel WD-repeat and disordered-region-rich proteins. *FEBS Lett.* **582**, 3515–3519.
15. Jasavala, R., Martinez, H., Thumar, J., Andaya, A., Gingras, A. C., Eng, J. K. *et al.* (2007). Identification of putative androgen receptor interaction protein modules: cytoskeleton and endosomes modulate androgen receptor signaling in prostate cancer cells. *Mol. Cell. Proteomics*, **6**, 252–271.
16. Endo, Y., Sugiyama, A., Li, S. A., Ohmori, K., Ohata, H., Yoshida, Y. *et al.* (2008). Regulation of clathrin-mediated endocytosis by p53. *Genes Cells*, **13**, 375–386.
17. Kirchhausen, T. (2000). Clathrin. *Annu. Rev. Biochem.* **69**, 699–727.
18. McPherson, P. S., Kay, B. K. & Hussain, N. K. (2001). Signaling on the endocytic pathway. *Traffic*, **2**, 375–384.
19. Royle, S. J., Bright, N. A. & Lagnado, L. (2005). Clathrin is required for the function of the mitotic spindle. *Nature*, **434**, 1152–1157.
20. Wakeham, D. E., Chen, C. Y., Greene, B., Hwang, P. K. & Brodsky, F. M. (2003). Clathrin self-assembly involves coordinated weak interactions favorable for cellular regulation. *EMBO J.* **22**, 4980–4990.
21. Ohmori, K., Endo, Y., Yoshida, Y., Ohata, H., Taya, Y. & Enari, M. (2008). Monomeric but not trimeric clathrin heavy chain regulates p53-mediated transcription. *Oncogene*, **27**, 2215–2227.
22. Huang, K. M., Gullberg, L., Nelson, K. K., Stefan, C. J., Blumer, K. & Lemmon, S. K. (1997). Novel functions of clathrin light chains: clathrin heavy chain trimerization is defective in light chain-deficient yeast. *J. Cell. Sci.* **110**, 899–910.
23. Royle, S. J. & Lagnado, L. (2006). Trimerisation is important for the function of clathrin at the mitotic spindle. *J. Cell. Sci.* **119**, 4071–4078.
24. Ota, N. & Agard, D. A. (2001). Binding mode prediction for a flexible ligand in a flexible pocket using multi-conformation simulated annealing pseudo crystallographic refinement. *J. Mol. Biol.* **314**, 607–617.
25. Chen, C. Y., Reese, M. L., Hwang, P. K., Ota, N., Agard, D. & Brodsky, F. M. (2002). Clathrin light and heavy chain interface: alpha-helix binding superhelix loops via critical tryptophans. *EMBO J.* **21**, 6072–6082.
26. Bochkareva, E., Kaustov, L., Ayed, A., Yi, G. S., Lu, Y., Pineda-Lucena, A. *et al.* (2005). Single-stranded DNA mimicry in the p53 transactivation domain interaction with replication protein A. *Proc. Natl Acad. Sci. USA*, **102**, 15412–15417.
27. Ashcroft, M., Taya, Y. & Vousden, K. H. (2000). Stress signals utilize multiple pathways to stabilize p53. *Mol. Cell. Biol.* **20**, 3224–3233.
28. Dautry-Varsat, A. (1986). Receptor-mediated endocytosis: the intracellular journey of transferrin and its receptor. *Biochimie*, **68**, 375–381.
29. Wettey, F. R., Hawkins, S. F., Stewart, A., Luzio, J. P., Howard, J. C. & Jackson, A. P. (2002). Controlled elimination of clathrin heavy-chain expression in DT40 lymphocytes. *Science*, **297**, 1521–1525.
30. Di Lello, P., Jenkins, L. M., Jones, T. N., Nguyen, B. D., Hara, T., Yamaguchi, H. *et al.* (2006). Structure of the Tfb1/p53 complex: insights into the interaction between the p62/Tfb1 subunit of TFIIH and the activation domain of p53. *Mol. Cell*, **22**, 731–740.
31. Hao, Z., Duncan, G. S., Chang, C. C., Elia, A., Fang, M., Wakeham, A. *et al.* (2005). Specific ablation of the apoptotic functions of cytochrome *c* reveals a differential requirement for cytochrome *c* and Apaf-1 in apoptosis. *Cell*, **121**, 579–591.
32. Jorgensen, W. L. & Tirado-Rives, J. (1988). The OPLS potential functions for proteins. Energy minimizations for crystals of cyclic peptides and crambin. *J. Am. Chem. Soc.* **110**, 1657–1666.

MOLECULAR AND CELLULAR BIOLOGY, Dec. 2008, p. 7126–7138 Vol. 28, No. 23
0270-7306/08/$08.00+0 doi:10.1128/MCB.00897-08

PML Activates Transcription by Protecting HIPK2 and p300 from SCF^{Fbx3}-Mediated Degradation▽†

Yutaka Shima,[1] Takito Shima,[1] Tomoki Chiba,[2] Tatsuro Irimura,[3] Pier Paolo Pandolfi,[4] and Issay Kitabayashi[1]*

Molecular Oncology Division, National Cancer Center Research Institute, 5-1-1 Tsukiji, Chuo-ku, Tokyo 104-0045, Japan[1]; Graduate School of Life and Environmental Sciences, University of Tsukuba, 1-1-1 Ten-noudai, Tsukuba, Ibaraki 305-8572, Japan[2]; Graduate School of Pharmaceutical Sciences, University of Tokyo, 7-3-1 Hongo, Bunkyo-ku, Tokyo 113-0033, Japan[3]; and Beth Israel Deaconess Medical Center and Harvard Medical School, 77 Avenue Louis Pasteur, Boston, Massachusetts 02115[4]

Received 5 June 2008/Returned for modification 7 July 2008/Accepted 12 September 2008

PML, a nuclear protein, interacts with several transcription factors and their coactivators, such as HIPK2 and p300, resulting in the activation of transcription. Although PML is thought to achieve transcription activation by stabilizing the transcription factor complex, little is known about the underlying molecular mechanism. To clarify the role of PML in transcription regulation, we purified the PML complex and identified Fbxo3 (Fbx3), Skp1, and Cullin1 as novel components of this complex. Fbx3 formed SCF^{Fbx3} ubiquitin ligase and promoted the degradation of HIPK2 and p300 by the ubiquitin-proteasome pathway. PML inhibited this degradation through a mechanism that unexpectedly did not involve inhibition of the ubiquitination of HIPK2. PML, Fbx3, and HIPK2 synergistically activated p53-induced transcription. Our findings suggest that PML stabilizes the transcription factor complex by protecting HIPK2 and p300 from SCF^{Fbx3}-induced degradation until transcription is completed. In contrast, the leukemia-associated fusion PML-RARα induced the degradation of HIPK2. We discuss the roles of PML and PML-retinoic acid receptor α, as well as those of HIPK2 and p300 ubiquitination, in transcriptional regulation and leukemogenesis.

In human leukemia, specific chromosomal translocations result in the expression of specific fusion proteins and malignancy (16, 39). The *PML* gene is the target of the t(15;17) chromosome translocation in acute promyelocytic leukemia (APL) and is fused to the retinoic acid receptor α (RARα) gene, which leads to the generation of a PML-RARα fusion protein (11, 12, 18, 28). The PML protein is known to localize in discrete nuclear speckles called PML nuclear bodies (NBs) (58). In the NBs, PML interacts with several transcription factors such as p53 and AML1, transcription coactivators such as HIPK2 and p300, and apoptosis modulators such as pRB and DAXX (27, 52, 53). PML enhances p53-dependent apoptosis by inducing p53 target genes (15, 20). Additionally, PML can lead to cell senescence by activating p53 (46). We have reported that PML interacts with AML1, a target of several chromosome translocations in leukemia (41), and stimulates the AML1-dependent differentiation of murine myeloid progenitor cells (44). APL-derived PML-RARα is thought to be dominant negative to PML. PML-RARα disrupts NBs into microspeckles (14) and inhibits DNA damage-induced apoptosis (56) and PML IV enhancement of PU.1-induced myeloid differentiation (57). Thus, PML activates and PML-RARα represses transcription. However, little is known about how PML activates transcription. Moreover, it remains unclear why transcription factors and coactivators are localized in NBs.

The ubiquitin-proteasome pathway involves two successive steps: labeling of the substrates with multiple ubiquitin molecules and degradation of the labeled substrates at the 26S proteasome. Ubiquitin conjugation is catalyzed by three enzymes: the ubiquitin-activating enzyme E1, the ubiquitin-conjugating enzyme E2, and the ubiquitin-protein ligase E3 (17). E3 ubiquitin ligases are classified into several types, including HECT-type E3, RING finger motif-containing E3, and U-box domain containing E3. MDM2, the APC/C complex, and the SCF complex are known to be the RING finger motif-containing E3 (21, 33, 54). The SCF complex is composed of F-box protein, Skp1, Cullin1 (Cul1), and ROC1. In the SCF complex, F-box proteins recognize specific substrates for ubiquitination. Therefore, the different SCF complexes are designated according to their F-box proteins (7, 24, 30). Proteins ubiquitinated by the SCF complex are degraded rapidly by the proteasome.

In this study, we purified the PML complex to clarify the role of PML in transcription and identified Fbxo3 (Fbx3), Skp1, and Cul1 as components of the PML complex. We found that Fbx3, whose substrates were unknown, formed SCF^{Fbx3} ubiquitin ligase and regulated the degradation of HIPK2 and p300 by the ubiquitin-proteasome pathway. This degradation was inhibited by PML through a mechanism that did not involve the inhibition of ubiquitination. PML, HIPK2, and Fbx3 increased p53 transcriptional activity synergistically. Our data suggest that the interplay between SCF^{Fbx3}-induced ubiquitination and degradation of transcription coactivators, such as HIPK2 and p300, and the stabilization of these coactivators by PML play critical roles in transcriptional regulation.

* Corresponding author. Mailing address: Molecular Oncology Division, National Cancer Center Research Institute, 5-1-1 Tsukiji, Chuo-ku, Tokyo 104-0045, Japan. Phone: 81 3 3547 5274. Fax: 81 3 3542 0688. E-mail: ikitabay@ncc.go.jp.

† Supplemental material for this article may be found at http://mcb.asm.org/.

▽ Published ahead of print on 22 September 2008.

MATERIALS AND METHODS

Cell culture, infection, and antibodies. K562 cells, MOLT-4 cells, H1299 cells, MCF7 cells, and NB4 cells were cultured in RPMI 1640 medium supplemented with 10% fetal calf serum (FCS). SKNO-1 cells were cultured in GIT (Wako). BOSC23 cells and PLAT-E cells were cultured in Dulbecco's modified Eagle's medium supplemented with 10% FCS. NIH 3T3 cells were cultured in Dulbecco's modified Eagle's medium supplemented with 10% calf serum. Mouse bone marrow (BM) cell suspensions were prepared by flushing isolated femora with phosphate-buffered saline (PBS), and the cells were cultured in StemPro-34 supplemented with 2.5% nutrient supplement, 2 mM L-glutamine, 10 ng/ml interleukin-3, 50 ng/ml SCF, 10 ng/ml oncostatin M, 20 ng/ml interleukin-6, 1% penicillin-streptomycin, and 0.1% tylosin. For the production of retroviruses, PLAT-E cells were transfected with pMSCV-derived retroviruses by the calcium phosphate precipitation method, and culture supernatants were collected 48 h after transfection. NIH 3T3 cells were infected by incubation in the culture supernatant of PLAT-E cells transfectants for 24 h.

Anti-HIPK2 antibody was described previously (26). Anti-Fbx3 antibody was generated by immunizing mice with glutathione *S*-transferase-tagged Fbx3. Other antibodies were purchased commercially and were as follows: antihemagglutinin (anti-HA) (3F10; Roche), anti-FLAG (M2; Sigma), anti-Gal4 (RK5C1; Santa Cruz), anti-p300 (N15; Santa Cruz), antitubulin (H235; Santa Cruz), antiubiquitin (FK2; Nippon Bio-Test), and anti-PML (001 [MBL], H238 [Santa Cruz], or 36.1-104 [UBI]).

Plasmids. Human Fbx3 cDNA was amplified by PCR from a human cDNA library generated from poly(A)$^+$ RNA of K562 cells by use of the oligonucleotides 5′-ACCGGGCCAGGCAAGATGGC-3′ as the upstream primer and 5′-GCAAACCCAAACAATCCAATTCC-3′ as the downstream primer. The N-terminal FLAG tag and HA tag were fused to Fbx3 cDNAs by use of the oligonucleotide 5′-ACGTACCGCGGACCATGGCAGACTACAAGGACGACGATGACAAGGCGGCCATGGAGACCGAGAC-3′ or 5′-ACGTACCGCGGACCATGGCATACCCATACGACGTGCCTGACTACGCTGCGGCCATGGAGACCGAGAC-3′ as the upstream primer and 5′-TCTGCGCTTCCACAGCATCG-3′ as the downstream primer in the PCR. Fbx3 deletion mutants were generated by PCR using pcDNA-HA-Fbx3 or pcDNA-FLAG-Fbx3 as the template. The PML, AML1, p300, and HIPK2 expression vectors were generated as described previously (1, 32, 37, 44, 57). p53 expression vectors and the MDM2-luc reporter were kindly provided by Y. Taya.

Purification of the PML complex. K562 cells were transfected with pLNCX or pLNCX-FLAG-PML I by electroporation. Cells stably expressing FLAG-PML I protein were cloned. The cells ($\sim 1 \times 10^{10}$ cells) were lysed by sonication at 4°C in 500 ml of 500 mM NaCl lysis buffer (20 mM sodium phosphate, pH 7.0, 500 mM NaCl, 30 mM sodium pyrophosphate, 0.1% NP-40, 5 mM EDTA, 10 mM NaF, 5 mM dithiothreitol [DTT], and 1 mM phenylmethylsulfonyl fluoride [PMSF]) supplemented with Complete (Roche). The lysates were cleared by centrifugation at 40,000 × *g* for 30 min at 4°C and incubated with 2.5 ml of anti-FLAG monoclonal antibody (M2)-conjugated beads with rotation at 4°C for 12 h. The beads with absorbed PML I immunocomplexes were washed six times with 50 ml of lysis buffer (20 mM sodium phosphate, pH 7.0, 250 mM NaCl, 30 mM sodium pyrophosphate, 0.1% NP-40, 5 mM EDTA, 10 mM NaF, 5 mM DTT, and 1 mM PMSF). The PML I complexes were selectively eluted by incubating twice with 0.2 mg/ml FLAG peptide in 7.5 ml of lysis buffer for 2 h. The eluates were concentrated using a filtration device and separated by sodium dodecyl sulfate-polyacrylamide gel electrophoresis (SDS-PAGE). Proteins were stained with Coomassie brilliant blue, excised, destained with 25 mM ammonium bicarbonate and 50% acetonitrile, dried, digested with sequence-grade modified trypsin in 50 mM Tris-HCl (pH 7.6), extracted with 5% trifluoroacetic acid-50% acetonitrile, and subjected to liquid chromatography-tandem mass spectrometry analysis.

Immunoprecipitation and Western blotting. BOSC23 cells were transfected with the desired vectors. After 15 h, culture supernatants were exchanged for fresh media and cells were treated with or without 10 μM MG132 (Calbiochem) for 9 h. The cells were lysed by incubation at 4°C for 30 min in lysis buffer. The lysates were cleared by centrifugation at 40,000 × *g* for 30 min at 4°C and the supernatants were incubated with anti-FLAG antibody-conjugated beads with rotation at 4°C for 12 h. The beads were washed six times with 1 ml of lysis buffer. After being washed, the cell extracts were selectively eluted by incubating with 0.2 mg/ml FLAG peptide for 2 h.

Cell lysates and immunoprecipitates were fractionated on SDS-polyacrylamide gels and transferred onto nitrocellulose membranes (Amersham). The membranes were incubated with primary antibodies and with horseradish peroxidase-conjugated secondary antibodies. The immune complexes were visualized by the ECL or ECL-Plus technique (Amersham).

RNA interference, RT-PCR, and real-time PCR. Fbx3-specific and control small interfering RNAs (siRNAs) were purchased from Ambion. RARα-specific and control stealth siRNAs were purchased from Invitrogen. MOLT-4 cells and NB4 cells were transfected with these siRNAs by using Nucleofector (Amaxa). NIH 3T3 cells were transfected five times with these siRNAs by use of Lipofectamine 2000. For reverse transcriptase PCR (RT-PCR), total RNA was purified using an RNeasy mini kit (Qiagen), and cDNAs were transcribed using SuperScript II RT (Invitrogen). PCRs were performed using the following primers: Fbx3 (human) forward (5′-GGTGTCCTCGGATGGTTTTATCTC-3′) and reverse (5′-TCTCTGATGATGGGGAAGCCAC-3′). Fbx3 (mouse) forward (5′-ACCCTCTGCTGCTCATCTTATCC-3′) and reverse (5′-CCACTAACTTTTGCCCGTTGTG-3′). HIPK2 forward (5′-GCTTCCAGCACAAGAACCACAC-3′) and reverse (5′-GCAATGACACAACCAAGGGACC-3′), p300 forward (5′-GCAATGGACAAAAAGGCAGTTC-3′) and reverse (5′-TGAGAGGAAGACACACAGGACAATC-3′), glyceraldehyde-3-phosphate dehydrogenase forward (5′-CTTCACCACCATGGAGAAGGC-3′) and reverse (5′-GGCATGGACTGTGGTCATGAG-3′), PML-RARα forward (5′-CCAATACAACGACAGCCCAGAAG-3′) and reverse (5′-CCATAGTGGTAGCCTGAGGACTTG-3′), and RARα forward (5′-CAGAACTGCTTGACCAAAGGACC-3′) and reverse (5′-AAGGCTTGTAGATGCGGGGTAGAG-3′). Real-time PCR was performed using the 7500 fast real-time PCR system (Applied Biosystems). The expression of the *p21* gene was normalized with respect to the expression of the *TBP* gene.

In vivo degradation assay. BOSC23 cells were transfected with the desired vectors, increasing amounts of pcDNA-HA-Fbx3, and pFA-CMV for expression of the Gal4 DNA-binding domain (Gal4 BD) as an internal control. After 24 h, the cells were lysed. The lysates were analyzed by Western blotting.

In vivo ubiquitination assay. BOSC23 cells were transfected with the desired vectors. Cells were treated with 50 μM MG132 1 h before harvesting and lysed in lysis buffer. To assay the stabilization of ubiquitinated HIPK2, cells were lysed in radioimmunoprecipitation assay buffer (20 mM Tris-HCl, pH 7.5, 150 mM NaCl, 2 mM EDTA, 0.25% SDS, 1% NP-40, 1% sodium deoxycholic acid, 5 mM DTT, and 1 mM PMSF) supplemented with Complete. The lysates were incubated with anti-FLAG antibody-conjugated beads as described above. Ubiquitinated HIPK2 was detected by immunoblotting with the antiubiquitin antibody, followed by treatment with horseradish peroxidase-conjugated secondary antibodies as described above.

Immunofluorescence. MCF7 cells were cultured in four-well chamber slides and transfected with pLNCX-FLAG-PML I and pcDNA-HA-Cul1, pcDNA-HA-Fbx3, or pcDNA-HA-Skp1, or pLNCX-FLAG-PML IV and pLNCX-HA-HIPK2 or pLNCX-HA-p300 by use of Lipofectamine 2000. The cells were treated with or without 10 μM MG132 for 18 h (HIPK2) or 9 h (p300). After MG132 treatment, the cells were fixed with 4% formaldehyde in PBS and incubated with 0.2% Triton X-100 in PBS for 5 min at room temperature. Antibodies were diluted in blocking buffer (1% FCS in PBS). Cells were incubated with the primary antibodies for 12 h at 4°C and then incubated with the secondary antibodies. The slides were mounted in Vectashield (Vector Laboratories). Images were captured on an Olympus microscope.

Luciferase assay. H1299 cells were transfected using the calcium phosphate precipitation method or Lipofectamine 2000 in 24-well plates, and luciferase activity was assayed after 24 h with a Veritas luminometer (Turner Biosystems) according to the manufacturer's protocol (Promega). Results of reporter assays are represented as the mean values for relative luciferase activity generated from four independent experiments and normalized against the activity of the enzyme form phRG-TK as an internal control.

RESULTS

PML complex contains Cul1, Fbx3, and Skp1. In order to clarify the role of PML in transcription, we purified the PML complex from the cell lysates of K562 cells expressing FLAG-tagged PML I and resolved the complex by SDS-PAGE. Liquid chromatography-tandem mass spectrometry analysis identified Cul1, Fbx3, and Skp1 as components of the PML complex (Fig. 1A and B). Other proteins identified in the PML complex are shown in Table S1 in the supplemental material. To test whether Cul1, Fbx3, or Skp1 interacts with PML I, we used immunofluorescence analysis. HA-tagged Cul1, HA-tagged Fbx3, or HA-tagged Skp1 was cotransfected with FLAG-tagged PML I into MCF7 cells, and the locations of these

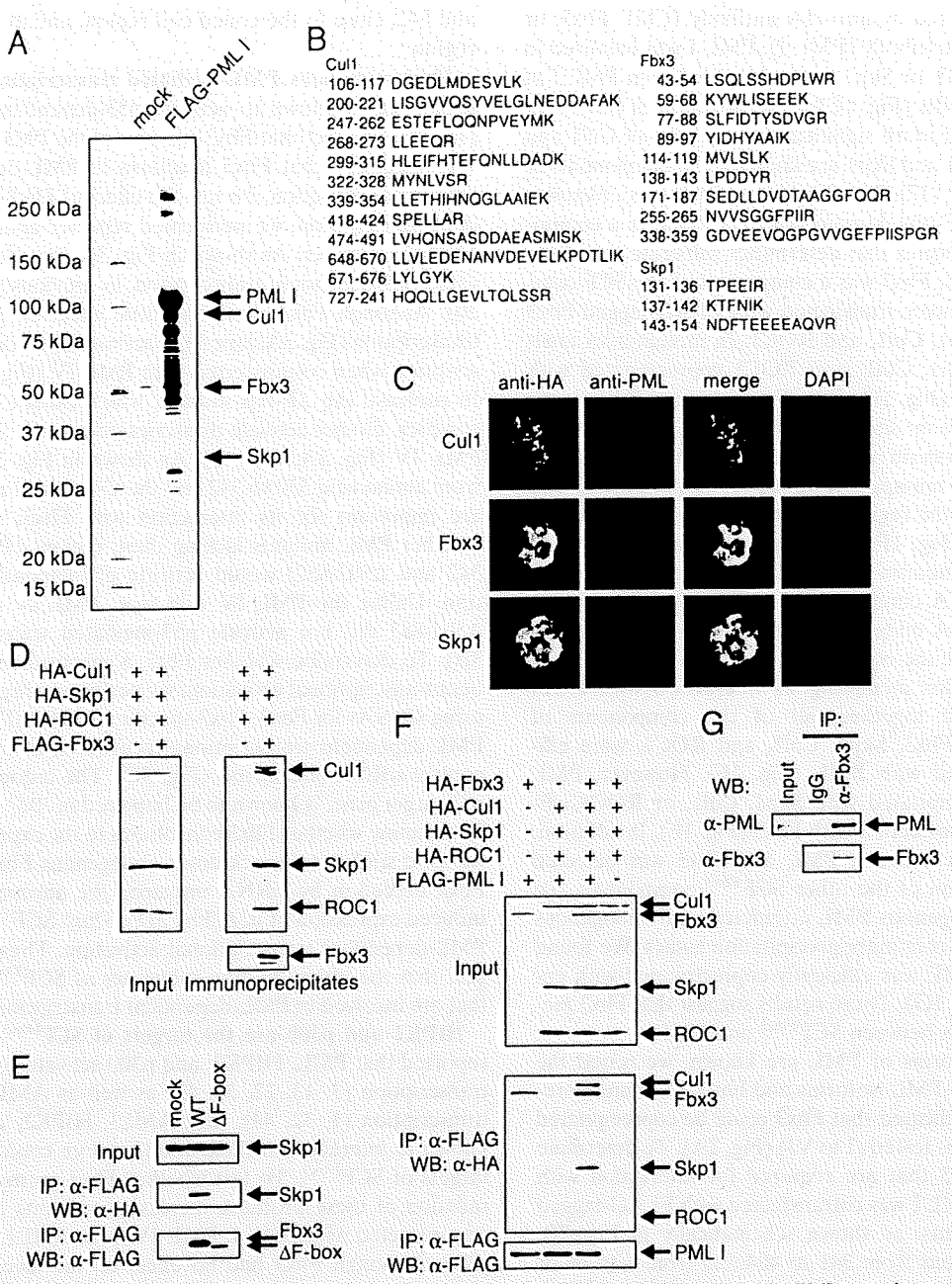

FIG. 1. Ubiquitin ligase SCF^{Fbx3} is part of the PML complex. (A) Purification of the PML complex. The PML complex was purified from cell lysates prepared from K562 cells carrying an empty vector (mock) or stably expressing FLAG-tagged PML I. The complexes were incubated with anti-FLAG antibody-conjugated agarose, and the bound materials were eluted with the FLAG peptide. The eluates were resolved by SDS-PAGE and visualized by silver staining. The proteins were identified by mass spectrometry. (B) The amino acid sequences of the peptides derived from the fractions specific to the FLAG-PML I-expressing cells. The proteins in the specific fractions were identified as Cul1, Fbx3, and Skp1. (C) Cul1, Fbx3, and Skp1 colocalized with PML I. MCF7 cells were cotransfected with pLNCX-FLAG-PML I and pcDNA-HA-Cul1, pcDNA-HA-Fbx3, or pcDNA-HA-Skp1. Cul1, Fbx3, and Skp1 were stained with anti-HA antibody and PML I was stained with anti-PML (001) antibody. DAPI, 4′,6′-diamidino-2-phenylindole. (D) Fbx3 forms a complex with Skp1, Cul1, and ROC1. BOSC23 cells were transfected with pcDNA-HA-Skp1, pcDNA-HA-Cul1, pcDNA-HA-ROC1, and either the empty vector (−) or pcDNA-FLAG-Fbx3. The expression of Skp1, Cul1, and ROC1 in the lysates of transfectants was detected by immunoblotting using anti-HA antibody (left). The Fbx3 complex was immunoprecipitated with anti-FLAG antibody. The immunoprecipitates were analyzed by immunoblotting using anti-HA and anti-FLAG antibodies (right). (E) The F-box domain is required for the interaction between Fbx3 and Skp1. BOSC23 cells were transfected with pcDNA-HA-Skp1 and either mock or pcDNA-FLAG-Fbx3 constructs as indicated. The expression of Skp1 in the lysates of transfectants was detected by immunoblotting using anti-HA antibody (top). The lysates of transfectants were incubated with anti-FLAG antibody. The immunoprecipitates were analyzed by immunoblotting using anti-HA (middle) and anti-FLAG (bottom) antibodies. (F) PML interacts with SCF^{Fbx3} through Fbx3. BOSC23 cells were cotransfected with pcDNA-HA-Fbx3, pcDNA-HA-Skp1, pcDNA-HA-Cul1, pcDNA-HA-ROC1, and either mock empty vector or pLNCX-FLAG-PML I. The interactions between PML I and components of SCF^{Fbx3} were analyzed as described for panel D. (G) Endogenous Fbx3 interacts with endogenous PML. SKNO-1 cells were lysed and Fbx3 was immunoprecipitated with anti-Fbx3 antibody. The immunoprecipitates were analyzed by immunoblotting with anti-Fbx3 and anti-PML (H238) antibodies. IP, immunoprecipitate; WB, Western blot; α-, anti-.

proteins were detected by anti-HA antibody (Cul1, Fbx3, or Skp1) or anti-PML antibody (PML I). PML I was localized in NBs, and Cul1, Fbx3, or Skp1 was colocalized with PML I at the peripheries of NBs (Fig. 1C). Colocalization of Fbx3 with PML I was detected more significantly than that of Cul1 and Skp1 (Fig. 1C). Cul1 and Skp1 are known to be components of SCF ubiquitin ligase (17). The function of Fbx3 was unknown, but it contains the F-box domain, which is found in a component of the SCF complex that determines substrate specificity (24). To confirm that Fbx3 was a component of the SCF complex, BOSC23 cells were transfected with FLAG-tagged Fbx3 and HA-tagged Skp1, Cul1, and ROC1. In immunoblot analysis, HA-tagged Skp1, Cul1, and ROC1 coprecipitated with FLAG-tagged Fbx3 (Fig. 1D). The F-box domain is known to be a Skp1 interaction site (30). Therefore, we examined whether the F-box domain of Fbx3 was required for interaction with Skp1. The Fbx3 mutant lacking the F-box domain (ΔF-box mutant; deletion of the region from 61 to 471) did not coprecipitate with Skp1 (Fig. 1E). These results suggest that Fbx3 can form an SCF ubiquitin ligase (SCF^{Fbx3}).

As shown in Fig. 1A, components of SCF^{Fbx3} were present in the PML complex. A coimmunoprecipitation assay was performed to determine the component of SCF^{Fbx3} that was primarily responsible for mediating its interaction with PML. When cotransfected together, all of the components of SCF^{Fbx3}, including Fbx3, Skp1, Cul1, and ROC1, were efficiently coprecipitated with PML (Fig. 1F). However, PML could not be coprecipitated with Skp1, Cul1, or ROC1 efficiently without cotransfection with Fbx3 (Fig. 1F). In addition, a strong interaction between PML and Fbx3 was detected without cotransfection of the other SCF^{Fbx3} components. To assess whether endogenous PML interacted with endogenous Fbx3, we performed coimmunoprecipitation assays. We found that endogenous PML was efficiently coprecipitated with endogenous Fbx3 (Fig. 1G). These results suggest that Fbx3 mediates the interaction between SCF^{Fbx3} and PML.

Since several isoforms of PML are known, we tested the interactions between PML isoforms and Fbx3. Coimmunoprecipitation analysis indicated that Fbx3 could be coprecipitated with all PML isoforms tested (I to VI) (Fig. 2A). To determine the domains in Fbx3 that are required for interaction with PML, HA-tagged PML I was cotransfected with FLAG-tagged Fbx3 deletion mutants, as shown schematically in Fig. 2B. Deletion of the regions from 341 to 404 and from 1 to 60 of Fbx3 are required for interaction with PML (Fig. 2C). The Fbx3 mutant (deletion of 61 to 340), which does not contain both regions, did not interact with PML I at all. To determine the domains in PML that are required for the interaction with Fbx3, FLAG-tagged Fbx3 was cotransfected with HA-tagged wild-type or truncated versions of PML, as shown schematically in Fig. 2D. Removal of the N-terminal proline-rich (Pro) region (1 to 55), the coiled-coil region (217 to 329), or the serine-proline region (502 to 553) did not affect the interaction with Fbx3. C-terminal deletions up to amino acid 343 did not affect the interaction, but further deletion up to 313 resulted in the loss of interaction (Fig. 2E). However, Fbx3 interacted with the PML mutant truncated between amino acids 330 and 342 (Fig. 2F). Fbx3 also interacted with the PML mutant with a truncation in its N-terminal region (Fig. 2F). Thus, the Fbx3 interaction sites of PML are located between amino acids 330 and 342, close to the coiled-coil region, and in the C-terminal region.

Fbx3 stimulates PML-mediated transcriptional activity of p53. PML is known to activate p53-dependent transcription (15, 20). The fact that Fbx3 is a part of the PML complex (Fig. 1A) suggested that Fbx3 functions in PML-dependent transcriptional activation. To test the effect of Fbx3 on p53-dependent transcription, we performed reporter analyses using the MDM2 promoter. As shown in Fig. 3A, lane 8, PML IV activated p53-dependent transcription, as previously reported (15, 20). Although Fbx3 alone had little effect on p53-dependent transcription (Fig. 3A, lane 9), it activated p53-dependent transcription when cotransfected with PML IV (Fig. 3A, lane 11). In contrast, the ΔF-box mutant, which cannot form the SCF complex, did not activate transcription even in the presence of PML IV (Fig. 3A, lane 12). As shown in Fig. 2E, the region from amino acid 330 to 342 and the C-terminal region of PML are important for its interaction with Fbx3. We examined whether PML mutants lacking these regions (PML IV Δ330-342 and Δ502-882) would activate p53-dependent transcription. Unlike the PML IV wild type, PML IV Δ330-342 and Δ502-882 did not activate p53-mediated transcription (Fig. 3B). To determine whether Fbx3 is involved in PML-dependent transcriptional activation, we performed reporter analyses using siRNAs for Fbx3. Fbx3-specific siRNA (siFbx3) inhibited PML-dependent transcriptional activation, in contrast to the control siRNA (siControl) (Fig. 3C). The induction of *p21*, a p53 target gene, is known to be impaired in $PML^{-/-}$ cells (20). To examine whether Fbx3 contributes to the expression of *p21*, we used siRNA to knock down endogenous Fbx3 expression. Fbx3 depletion by siRNA impaired the adriamycin (ADR)-induced expression of *p21* (Fig. 3D). Thus, SCF^{Fbx3} stimulates PML-dependent transcriptional activation. These results suggest that the ubiquitination substrates of SCF^{Fbx3} are factors that are involved in PML-dependent transcriptional activation.

HIPK2 and p300 are the targets of SCF^{Fbx3}. It has been reported that PML, HIPK2, and p300 activate p53-dependent transcription (3, 13, 22, 38, 42) as well as AML1-dependent transcription (1, 32, 44). p53, AML1, HIPK2, and p300 are known to interact with PML and therefore could be potential targets of SCF^{Fbx3}. To test whether Fbx3 promoted the degradation of these proteins, increasing amounts of Fbx3 were cotransfected with PML I, PML IV, p53, AML1, HIPK2, and p300. Although Fbx3 had no effect on the levels of PML I, PML IV, p53, or AML1 (Fig. 4A), it decreased the levels of HIPK2 and p300 in a dose-dependent manner (Fig. 4A). These decreases were inhibited by the proteasome inhibitor MG132 (Fig. 4A). The ΔF-box mutant did not decrease the levels of either HIPK2 or p300 (Fig. 4B). To examine whether endogenous HIPK2 and p300 were degraded by Fbx3, NIH 3T3 cells were infected with an empty retrovirus or a retrovirus encoding Fbx3 and cultured in the absence or presence of MG132. Immunoblot analysis indicated that Fbx3 overexpression decreased the levels of endogenous HIPK2 and p300 in the absence of MG132 but not in the presence of MG132 (Fig. 4C). These results suggest that SCF^{Fbx3} induces a proteasome-dependent degradation of HIPK2 and p300.

To determine whether endogenous HIPK2 and p300 were degraded by endogenous SCF^{Fbx3}, we used siRNA to knock down endogenous Fbx3 expression. Transfection of NIH 3T3

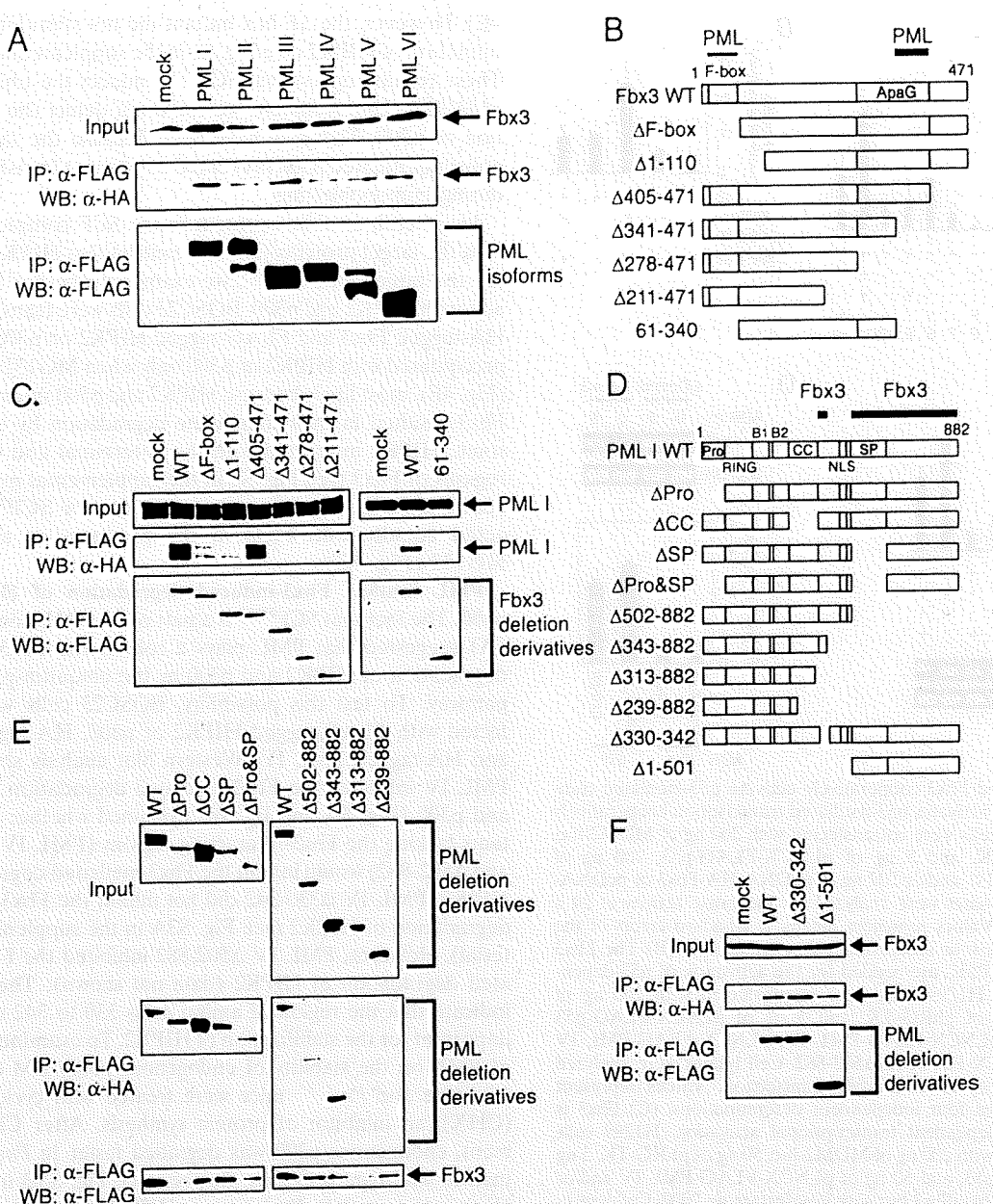

FIG. 2. PML and Fbx3 interact with their respective specific domains. (A) PML isoforms interact with Fbx3. BOSC23 cells were transfected with pLNCX-HA-Fbx3 and either mock or pLNCX-FLAG-PML isoforms (I to VI). The expression of Fbx3 in the lysates of transfectants was detected by immunoblotting using anti-HA antibody (top). The lysates of transfectants were incubated with anti-FLAG antibody. The immunoprecipitates were analyzed by immunoblotting using anti-HA (middle) and anti-FLAG (bottom) antibodies. (B) Schematic diagram of the structures of Fbx3 deletion mutants. PML indicates the strongly interacting (thick line) and weakly interacting (thin line) regions of Fbx3 as determined for panel C. (C) Identification of Fbx3 regions required for interaction with PML. BOSC23 cells were transfected with pLNCX-HA-PML I and mock or pcDNA-FLAG-Fbx3 deletion constructs as indicated. The expression of PML I in the lysates of transfectants was detected by immunoblotting using anti-HA antibody (top). The lysates of transfectants were incubated with anti-FLAG antibody. The immunoprecipitates were analyzed by immunoblotting using anti-HA (middle) and anti-FLAG (bottom) antibodies. (D) Schematic diagram of the structures of PML deletion mutants. The proline-rich region (Pro), the RING finger domain (RING), B-box domain 1 (B1), B-box domain 2 (B2), the coiled-coil domain (CC), the nuclear import signal (NLS), and the serine-proline-rich region (SP) are indicated. Fbx3 indicates the interacting region of PML as determined for panels E and F. (E and F) Identification of PML regions required for interaction with Fbx3. BOSC23 cells were cotransfected with pLNCX-FLAG-Fbx3 and pLNCX-HA-PML deletion constructs (E) or with pcDNA-HA-Fbx3 and pLNCX-FLAG-PML deletion constructs (F) as indicated. The interactions between Fbx3 and the PML mutants were analyzed as described for panel C. IP, immunoprecipitate; WB, Western blot; WT, wild type; α-, anti-.

cells with Fbx3 siRNA resulted in a decrease in Fbx3 mRNA levels (Fig. 4D, top). Fbx3 depletion by siRNA did not affect HIPK2 and p300 mRNA levels (Fig. 4D, top) but rather increased HIPK2 and p300 protein levels (Fig. 4D, bottom). These data demonstrate that the stability of HIPK2 and p300 is regulated by SCF^{Fbx3}.

In order to clarify whether SCF^{Fbx3} degrades HIPK2 by the ubiquitin-proteasome pathway, we examined whether Fbx3 in-

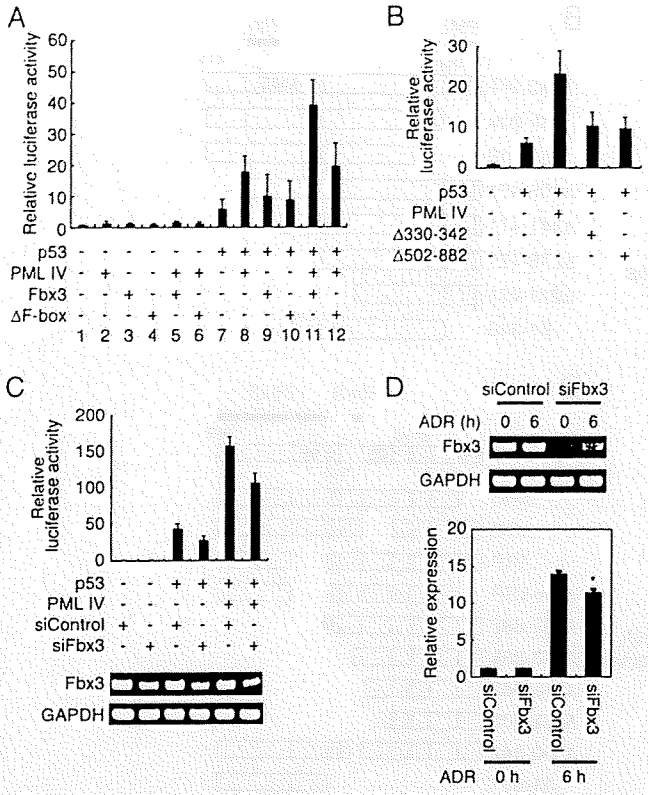

FIG. 3. PML and Fbx3 cooperatively activate p53-mediated transcription. (A) Fbx3 activates p53-mediated transcription cooperatively with PML. H1299 cells were cotransfected with 200 ng of MDM2-luc, 50 ng of phRG-TK, and 5 ng of pLNCX-FLAG-p53, 100 ng of pLNCX-HA-PML IV, and/or 200 ng of pcDNA-HA-Fbx3 or pcDNA-HA-ΔF-box. Cell lysates were analyzed for luciferase activity at 24 h after transfection. Values represent means ± standard errors of the means (SEM) from four independent determinations. (B) The Fbx3 interaction sites of PML are needed for the activation of p53-dependent transcription. H1299 cells were cotransfected with 200 ng of MDM2-luc, 50 ng of phRG-TK, and 5 ng of pLNCX-FLAG-p53 and/or 100 ng of pLNCX-FLAG-PML IV, pLNCX-FLAG-PML IV Δ330-342, or pLNCX-HA-PML Δ502-882. Cell lysates were analyzed for luciferase activity at 24 h after transfection. Values represent means ± SEM from four independent determinations. (C) Fbx3 is involved in PML-dependent transcriptional activation. H1299 cells were cotransfected with 200 ng of MDM2-luc, 50 ng of phRG-TK, 5 ng of pLNCX-FLAG-p53, and 50 ng of pLNCX-FLAG-PML IV and/or 100 pmol siControl or siFbx3 by using Lipofectamine 2000. Cell lysates were analyzed for luciferase activity at 24 h after transfection. Values represent means ± SEM from four independent determinations (top). The primers for RT-PCR (bottom) are described in Materials and Methods. (D) Expression of *p21* is decreased by knocking down Fbx3. MOLT-4 cells were transfected with siControl or siFbx3 and then treated with 0.5 μM ADR. The primers for RT-PCR (top) are described in Materials and Methods. The expression of *p21* was analyzed by real-time PCR (bottom). Values represent means ± SEM from four independent determinations. *, *P* value of <0.001 compared with the siControl value for the 6-h time point. GAPDH, glyceraldehyde-3-phosphate dehydrogenase.

duced the ubiquitination of HIPK2. BOSC23 cells were transfected with FLAG-tagged HIPK2 and HA-tagged Fbx3 and then treated with MG132. HIPK2 proteins were immunoprecipitated with anti-FLAG antibody. Western blot analysis of the immunoprecipitates by use of antiubiquitin antibody indicated that Fbx3 stimulated the ubiquitination of HIPK2 (Fig. 4E). However, the ΔF-box mutant did not stimulate the ubiquitination of HIPK2 (see Fig. S1 in the supplemental material). These results suggest that SCF^{Fbx3} induces the ubiquitination of HIPK2. Unfortunately, we could not detect the ubiquitination of p300. This may have been because the large size of polyubiquitinated p300 prevented its efficient transfer to filters during immunoblotting.

In general, an F-box protein in the SCF complex interacts with the target proteins (30). To confirm that HIPK2 and p300 are the targets of SCF^{Fbx3}, we examined whether Fbx3 interacts with HIPK2 and p300. BOSC23 cells were transfected with HA-tagged Fbx3 and FLAG-tagged HIPK2 or p300. Fbx3 coprecipitated with HIPK2 or p300 only when MG132 was added (Fig. 4F), most likely because HIPK2 and p300 interaction with Fbx3 resulted in their immediate degradation by the proteasome. HIPK2 interacted with the N-terminal and C-terminal regions of Fbx3 (see Fig. S2 in the supplemental material). In contrast, PML, which is not a substrate for SCF^{Fbx3}, interacted equally with Fbx3 in the presence or absence of MG132 (Fig. 4G).

PML inhibits Fbx3-induced degradation of HIPK2 and p300. The fact that SCF^{Fbx3} is a part of the PML complex (Fig. 1A) suggested that PML plays a role in the Fbx3-mediated degradation of HIPK2 and p300 by the ubiquitin-proteasome pathway. To test this possibility, BOSC23 cells were transfected with FLAG-tagged HIPK2 or p300, HA-tagged Fbx3, and HA-tagged PML IV. Western blot analysis showed that PML IV inhibited the Fbx3-mediated degradation of HIPK2 and p300 (Fig. 5A and B). We examined whether PML mutants lacking the Fbx3-interacting regions (PML IV Δ330-342 and Δ502-882) would inhibit the Fbx3-mediated degradation of HIPK2. PML IV Δ330-342 did not inhibit the Fbx3-mediated degradation of HIPK2 (see Fig. S3A in the supplemental material). However, PML IV Δ502-882 inhibited the Fbx3-mediated degradation of HIPK2 (data not shown). These results indicate that the region of amino acids 330 to 342 of PML is important for the stabilization of HIPK2. To examine the effect of PML on the stability of endogenous p300, BM cells from wild-type and $Pml^{-/-}$ mice were treated with cycloheximide (CHX), an inhibitor of protein synthesis. After CHX treatment, endogenous p300 was degraded faster in $Pml^{-/-}$ cells than in wild-type cells (Fig. 5C; also see Fig. S3B in the supplemental material). Endogenous HIPK2 was not detected in wild-type or $Pml^{-/-}$ BM cells or in murine embryonic fibroblasts (data not shown). These data suggest that PML stabilizes p300 by inhibiting its SCF^{Fbx3}-mediated degradation.

PML is known to accumulate in NBs together with many other proteins, such as HIPK2 and p300. We hypothesized that PML might stabilize HIPK and p300 by sequestering them in NBs away from ubiquitin-proteasome-related proteins in the nucleus. We used immunofluorescence analysis to test this hypothesis. HA-tagged HIPK2 or HA-tagged p300 was cotransfected with FLAG-tagged PML IV into MCF7 cells, and the locations of these proteins were detected by anti-HA antibody and anti-PML antibody, respectively. Without cotransfection with PML, HIPK2 was localized in microspeckles and p300 showed a diffuse staining pattern in the nucleus (Fig. 5D). When coexpressed with PML IV, HIPK2 and p300 colocalized with PML IV in NBs (Fig. 5E). When HIPK2 and p300 were cotransfected with PML IV, followed by treatment with

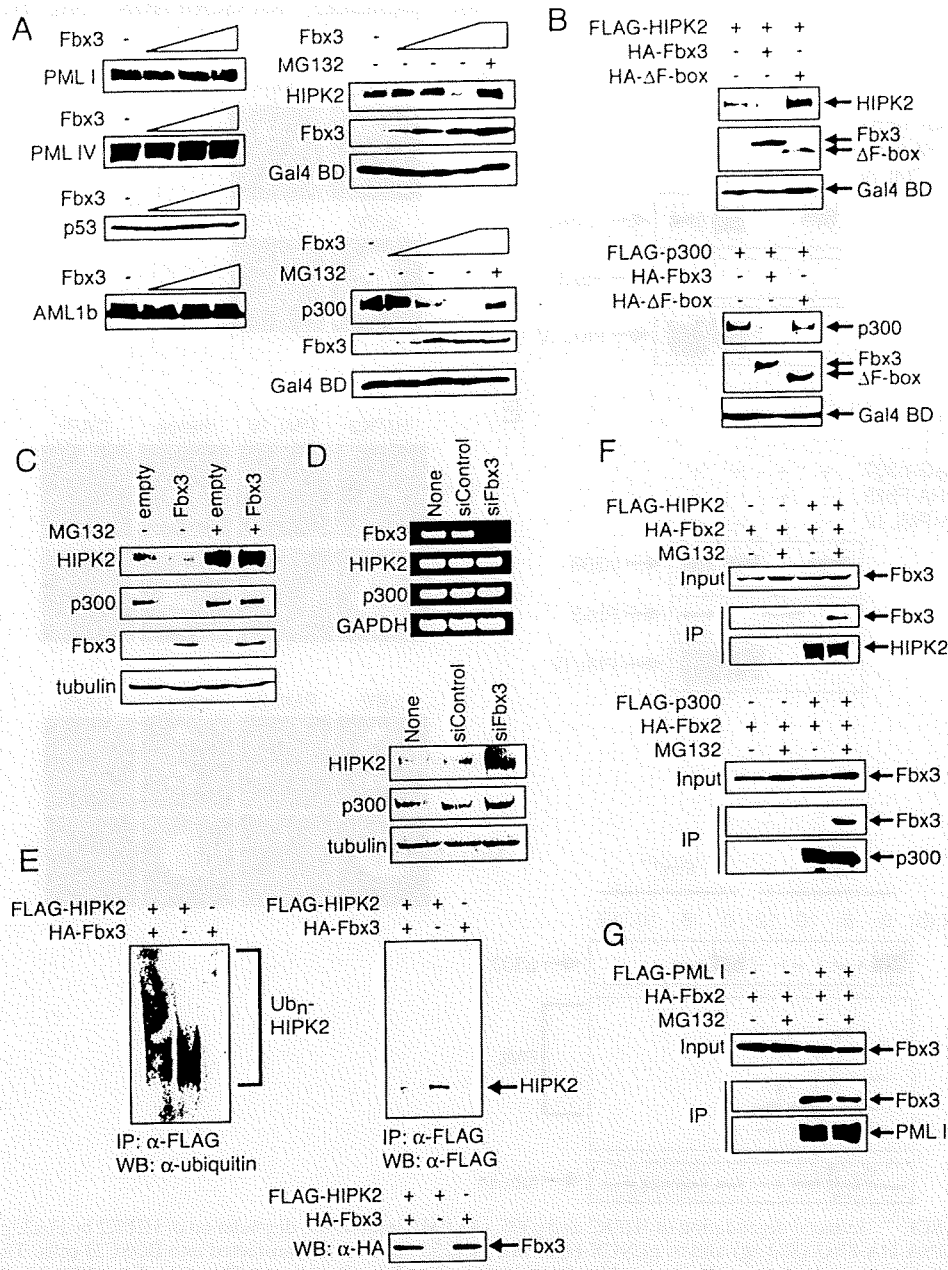

FIG. 4. HIPK2 and p300 are the targets of SCF^{Fbx3}. (A) Fbx3 induces the degradation of HIPK2 and p300. BOSC23 cells were cotransfected with 200 ng of pLNCX-FLAG-PML I, pLNCX-FLAG-PML IV, pLNCX-FLAG-p53, pLNCX-FLAG-AML1b, pLNCX-FLAG-HIPK2, or pLNCX-FLAG-p300; 100 ng of pFA-CMV for the expression of Gal4 BD as an internal control; and increasing amounts of pcDNA-HA-Fbx3 (0, 50, 200, and 800 ng). The expression of PML I, PML IV, p53, AML1, HIPK2, or p300 in the lysates of transfectants was detected by immunoblotting using anti-FLAG antibody. The expression of Fbx3 and Gal4 BD in the lysates of transfectants was detected by immunoblotting using anti-HA and anti-Gal4 antibodies, respectively. MG132 was added as described in Materials and Methods. (B) The F-box domain of Fbx3 is essential for the degradation of HIPK2 and p300. BOSC23 cells were cotransfected with pLNCX-FLAG-HIPK2 or pLNCX-FLAG-p300, pcDNA-HA-Fbx3 or pcDNA-HA-ΔF-box, and pFA-CMV. The cell lysates were analyzed as described for panel A. (C) Overexpression of Fbx3 induces the degradation of endogenous HIPK2 and p300. NIH 3T3 infectants with an empty retrovirus (empty) or a retrovirus encoding Fbx3, cultured in the absence or presence of MG132, were lysed in SDS-PAGE sample buffer. The expression of HIPK2, p300, Fbx3, and tubulin was detected by immunoblotting using anti-HIPK2, anti-p300, anti-HA, and antitubulin antibodies, respectively. (D) Expression of HIPK2 and p300 is increased by knocking down Fbx3. NIH 3T3 cells were transfected with siControl or siFbx3 five times. The primers for the RT-PCR (top) are described in Materials and Methods. The expression of HIPK2, p300, and tubulin was analyzed by Western blotting (bottom) using anti-HIPK2, anti-p300, and antitubulin, respectively. GAPDH, glyceraldehyde-3-phosphate dehydrogenase. (E) Fbx3 ubiquitinates HIPK2. BOSC23 cells were transfected with the desired vectors. Cells were treated with 50 μM MG132 and lysed. The lysates were immunoprecipitated with anti-FLAG antibody as described in Materials and Methods. The ubiquitination of HIPK2 was analyzed by immunoblotting using antiubiquitin. (F) HIPK2 and p300 interact with Fbx3 in the presence of MG132. BOSC23 cells were cotransfected with pcDNA-HA-Fbx3 and mock empty vector, pLNCX-FLAG-HIPK2 (top), or pLNCX-FLAG-p300 (bottom). Cells were treated with or without 10 μM MG132 for 9 h. The expression of Fbx3 in the lysates of transfectants was detected by immunoblotting using anti-HA antibody (Input). The lysates of transfectants were incubated with anti-FLAG antibody. The immunoprecipitates were analyzed by immunoblotting using anti-HA antibodies (middle) and anti-FLAG antibodies (bottom). (G) PML interacts with Fbx3. BOSC23 cells were transfected with pcDNA-HA-Fbx3 and either mock empty vector or pLNCX-FLAG-PML I. The interaction between Fbx3 and PML I was analyzed as described for panel F. IP, immunoprecipitate; WB, Western blot; α-, anti-.

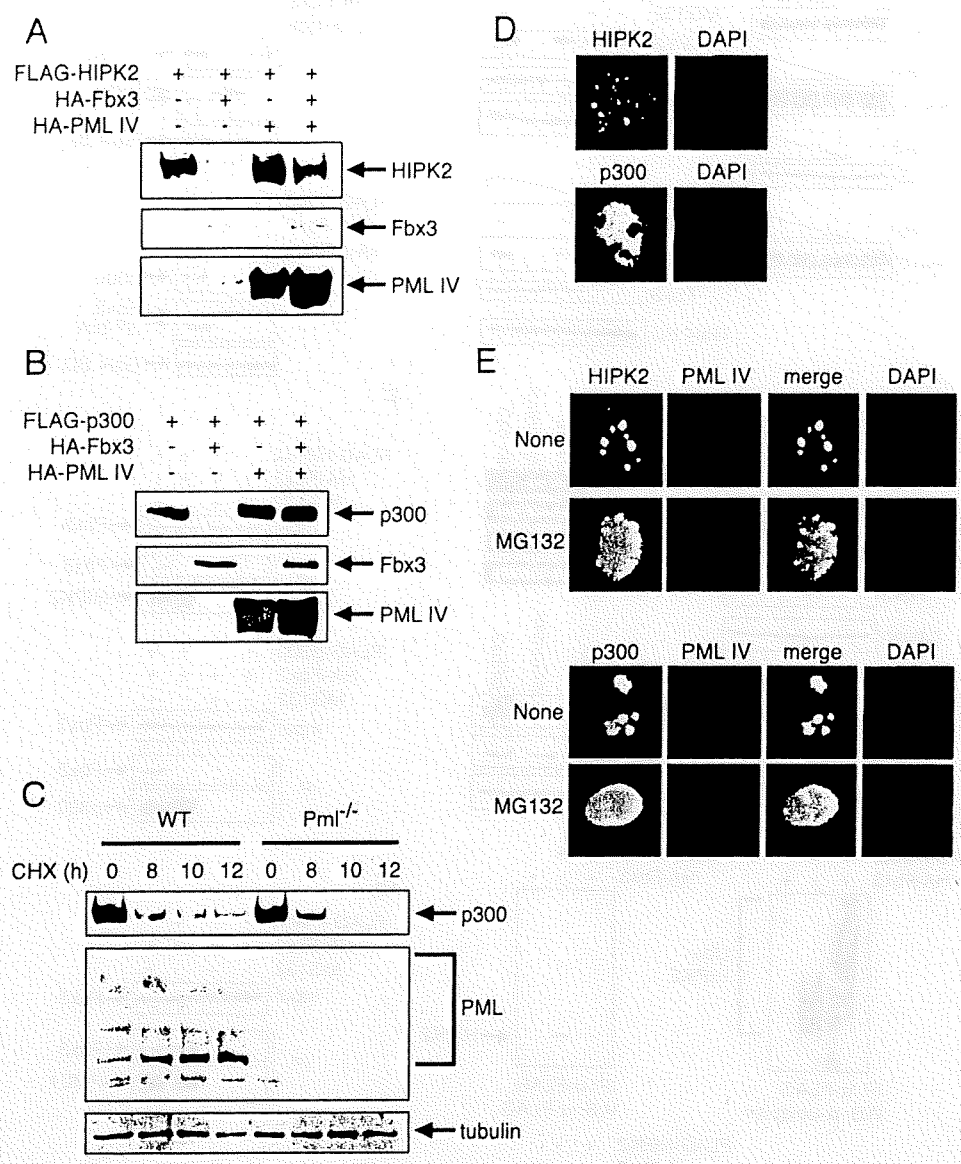

FIG. 5. PML inhibits SCF^{Fbx3}-induced degradation of HIPK2 and p300. (A) PML inhibits the degradation of HIPK2 by Fbx3. pLNCX-FLAG-HIPK2 (200 ng) and pcDNA-HA-Fbx3 (800 ng) and/or pLNCX-HA-PML IV (250 ng) were cotransfected into BOSC23 cells. The expression of HIPK2 in the lysates of transfectants was detected by immunoblotting using anti-FLAG antibody (top). The expression of Fbx3 (middle) and PML IV (bottom) in the lysates of transfectants was detected by immunoblotting using anti-HA antibody. (B) PML inhibits the degradation of p300 by Fbx3. pLNCX-FLAG-p300 (200 ng) and pcDNA-HA-Fbx3 (800 ng) and/or pLNCX-HA-PML IV (200 ng) were cotransfected into BOSC23 cells. The expression of p300 (top), Fbx3 (middle), and PML IV (bottom) was detected as described for panel A. (C) PML stabilizes p300. Wild-type (WT) and *Pml*$^{-/-}$ BM cells were treated with 100 μg/ml CHX. The expression of p300, PML, and tubulin was detected by immunoblotting using anti-p300, anti-PML (36.1-104), and antitubulin antibodies, respectively. (D) Localization of HIPK2 and p300 in the nucleus. MCF7 cells were transfected with pLNCX-HA-HIPK2 or pLNCX-HA-p300. The localization of HIPK2 and p300 was analyzed by use of anti-HA antibody. (E) HIPK2 and p300 are localized outside of NBs in the presence of MG132. MCF7 cells were cotransfected with pLNCX-FLAG-PML IV and pLNCX-HA-HIPK2 or pLNCX-HA-p300. Cells were treated with or without 10 μM MG132. HIPK2 and p300 were stained with anti-HA antibody and PML IV was stained with anti-PML (001) antibody. DAPI, 4′,6′-diamidino-2-phenylindole.

MG132, HIPK2 and p300 were localized to both the inside and outside of NBs. In contrast, PML was localized only in NBs before and after treatment with MG132 (Fig. 5E). Thus, MG132 stabilized HIPK2 and p300 outside of the NBs but not in the NBs. These results suggest that HIPK2 and p300 are degraded by the ubiquitin-proteasome pathway when located outside of NBs and stabilized by PML when located within NBs.

PML does not inhibit the ubiquitination of HIPK2 by SCF^{Fbx3}. PML inhibited the degradation of HIPK2 by SCF^{Fbx3} (Fig. 5A). To test whether PML affects the Fbx3-induced ubiquitination of HIPK2, BOSC23 cells were cotransfected with FLAG-tagged HIPK2, HA-tagged Fbx3, and HA-tagged PML IV. Without proteasome inhibitors, Fbx3 induced the degradation of HIPK2 (Fig. 6A, lane 3), and PML inhibited this degradation of HIPK2 (Fig. 6A, lane 4). However, the levels of

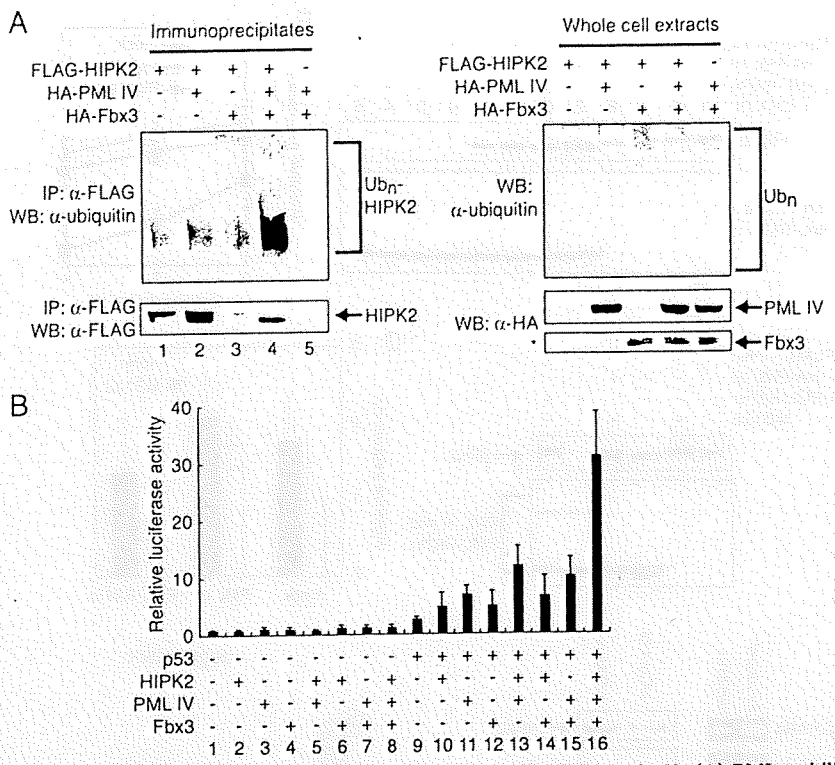

FIG. 6. PML stabilization of ubiquitinated HIPK2 is related to the transcriptional activity of p53. (A) PML stabilizes ubiquitinated HIPK2. BOSC23 cells were transfected with pLNCX-FLAG-HIPK2 and/or pcDNA-HA-Fbx3 and/or pLNCX-HA-PML IV. Cells were lysed as described in Materials and Methods. The immunoprecipitates by anti-FLAG antibody were analyzed by immunoblotting using antiubiquitin antibody. The asterisk indicates a nonspecific band present in all samples. (B) HIPK2, PML, and Fbx3 activate p53-dependent transcription synergistically. H1299 cells were cotransfected with 200 ng of MDM2-luc, 50 ng of phRG-TK, and 2.5 ng of pLNCX-FLAG-p53 or 700 ng of pLNCX-HA-HIPK2, 100 ng of pLNCX-HA-PML IV, and/or 200 ng of pcDNA-HA-Fbx3 as indicated. Cell lysates were analyzed for luciferase activity at 24 h after transfection. Values represent means ± SEM from four independent determinations. IP, immunoprecipitate; WB, Western blot; α-, anti-.

ubiquitinated HIPK2 were increased when HIPK2 was cotransfected together with both PML and Fbx3 (Fig. 6A, lane 4). These results suggest that PML inhibits the degradation of HIPK2 through a mechanism that does not involve the inhibition of its ubiquitination by SCF^{Fbx3}.

It has been reported that HIPK2 activates p53-dependent transcription (13, 22). To clarify the roles of HIPK2, PML IV, and Fbx3 in p53-dependent transcription, we performed reporter analyses using the MDM2 promoter with H1299 cells. HIPK2 increased p53 transcriptional activity (Fig. 6B, lane 10) as previously reported. Furthermore, HIPK2 and PML IV activated p53-mediated transcription cooperatively (Fig. 6B, lane 13). Since Fbx3 promotes the degradation of HIPK2, we initially thought that Fbx3 might inhibit the activation of p53-dependent transcription by HIPK2 and PML IV. However, Fbx3 stimulated this transcriptional activation (Fig. 6B, lane 16). These results are consistent with the results in Fig. 3A, which show that Fbx3 increases PML IV-mediated p53 transcriptional activity. Thus, HIPK2, PML IV, and Fbx3 activate p53-dependent transcription synergistically.

PML-RARα destabilizes HIPK2. PML-RARα is known to be a dominant-negative form of PML (49, 57). Therefore, we hypothesized that PML-RARα would not stabilize HIPK2. To test whether PML-RARα affects the stability of HIPK2, FLAG-tagged HIPK2 was mock transfected or cotransfected with PML IV or PML-RARα. As shown in Fig. 7A, the levels of HIPK2 did not decrease when it was cotransfected with PML IV. In contrast, the levels of HIPK2 decreased when it was transfected with PML-RARα. The stability of HIPK2 was also decreased by PML-RARα (Fig. 7B). This decrease in HIPK2 levels was rescued by adding MG132 (Fig. 7C and D). These data indicate that PML-RARα promotes the degradation of HIPK2 in a ubiquitin-proteasome-dependent manner. HIPK2 levels also decreased when it was cotransfected with the PML-RARα mutant truncated between amino acids 330 and 342 (see Fig. S4 in the supplemental material). To examine whether PML-RARα destabilizes endogenous HIPK2, we used siRNA for RARα to knock down PML-RARα expression in APL-derived NB4 cells. PML-RARα depletion increased the expression of endogenous HIPK2 (Fig. 7E). These results suggest that PML-RARα enhances HIPK2 degradation not by directly binding to Fbx3 but by inhibiting PML's stabilization of HIPK2.

DISCUSSION

HIPK2 and p300 are novel targets of SCF^{Fbx3}. In this study, we identified Fbx3 as a PML-interacting protein and as a subunit of SCF ubiquitin ligase that promoted the degradation of HIPK2 by the ubiquitin-proteasome pathway. Recently, Rinaldo and coworkers showed that MDM2 induced the degradation of HIPK2 in response to cytostatic doses of ADR or

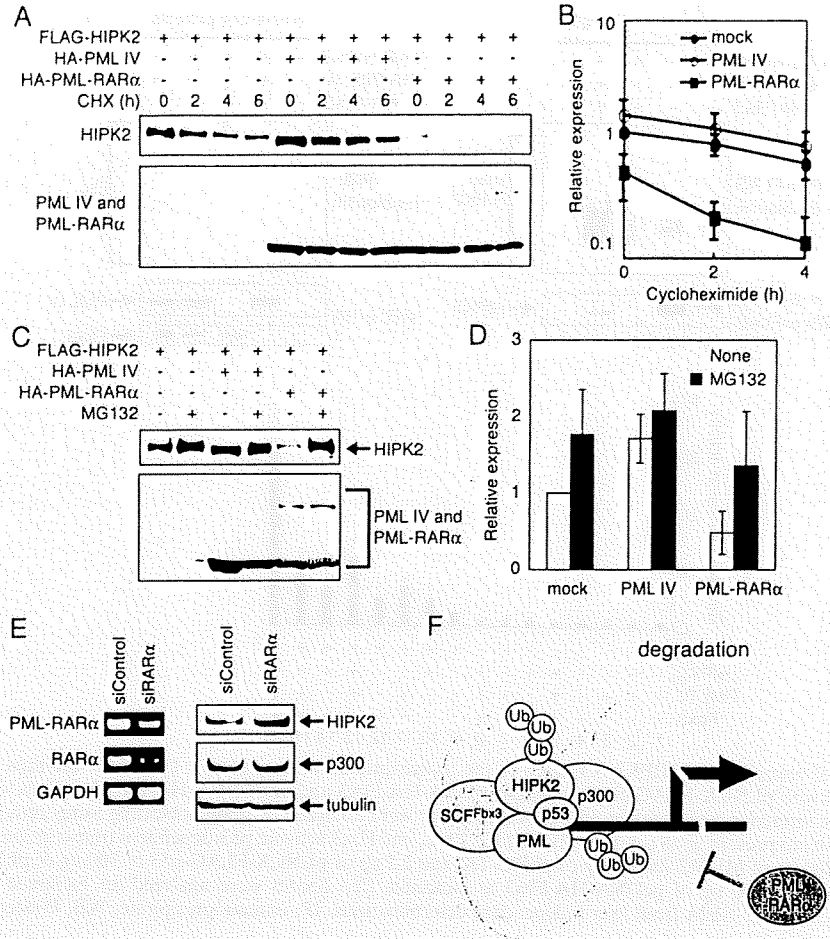

FIG. 7. PML-RARα destabilizes HIPK2. (A) PML-RARα enhances the degradation of HIPK2. BOSC23 cells were transfected with the appropriate vectors. Cells were treated with 100 μg/ml CHX and lysed. The expression of HIPK2 (top) and PML IV or PML-RARα (bottom) was detected by immunoblotting using anti-FLAG and anti-HA antibodies, respectively. (B) Quantitative analysis of HIPK2 levels following CHX treatment. Values were normalized to the mock value at the zero time point. Values represent means ± SEM from four independent determinations. (C) PML-RARα promotes the degradation of HIPK2 by the ubiquitin-proteasome pathway. BOSC23 cells were transfected with the appropriate vectors. Cells were treated with 10 μM MG132 and lysed. The lysates were analyzed as described for panel A. (D) Quantitative analysis of HIPK2 levels following MG132 treatment. Values were normalized to the nontreated mock value. Values represent means ± SEM from four independent determinations. (E) PML-RARα depletion increases the expression of HIPK2. NB4 cells were transfected with siControl or RARα-specific siRNA (siRARα). The primers for RT-PCR (left) are described in Materials and Methods. The expression of HIPK2, p300, and tubulin was analyzed by Western blot analysis (right) using anti-HIPK2, anti-p300, and antitubulin antibodies, respectively. GAPDH, glyceraldehyde-3-phosphate dehydrogenase. (F) A model for PML-mediated transcriptional activation. HIPK2 and p300 are the targets of SCF^{Fbx3}. Without PML, SCF^{Fbx3} degrades HIPK2 and p300 by the ubiquitin-proteasome pathway. PML stabilizes HIPK2 and p300 and inhibits their SCF^{Fbx3}-induced degradation. This stabilization of transcription coactivators by PML may activate transcription. PML-RARα acts as a dominant-negative inhibitor and destabilizes transcription coactivators. Ub, ubiquitin.

UV irradiation and that the C-terminal region of HIPK2 is critical for this degradation (50). Gresko and coworkers showed that the sumoylation of human HIPK2 at lysine 25 increased its stability (19). However, in this study, we found that Fbx3 could degrade mutants of HIPK2 deleted for the C-terminal region containing the lysine residue required for MDM2-mediated degradation, as well as the kinase-dead mutant (mutation of lysine 221 to alanine) and the HIPK2 K25R mutant, which cannot be sumoylated (see Fig. S5B in the supplemental material), and that Fbx3 depletion by siRNA did not inhibit the repression of HIPK2 by ADR (see Fig. S5C in the supplemental material). These data suggest that the N-terminal region of HIPK2, but not the C-terminal region, is necessary for SCF^{Fbx3}-induced degradation. Although we were unable to identify which lysine residue(s) is necessary for ubiquitination and degradation by SCF^{Fbx3}, it appears that HIPK2 degradation by SCF^{Fbx3} is different from MDM2-induced degradation and does not require lysine 25.

The degradation of p300 via the 26S proteasome pathway has previously been reported (6, 36, 48). This degradation appears to be dependent on p300 phosphorylation and dephosphorylation (9, 47). Doxorubicin-activated p38 mitogen-activated protein kinase phosphorylates p300 and induces p300 degradation (47). Protein phosphatase 2A, a serine-threonine phosphatase, also plays an important role in p300 degradation (9). Our data show that p300 is degraded by SCF^{Fbx3} via the 26S proteasome pathway, although it is unclear which modification of p300 mediates this degradation. Nonetheless, Fbx3

interacted with a form of p300 that had a faster electrophoretic mobility on SDS-polyacrylamide gels in the presence of MG132 (data not shown), suggesting that SCF^{Fbx3} recognizes and degrades dephosphorylated p300.

PML stimulates transcription by stabilizing HIPK2 and p300. PML has been suggested to play a role in the transcription of target genes that are regulated by transcription factors such as p53. However, the underlying mechanism has remained unclear. Our results suggest that PML stimulates transcription by protecting transcription coactivators such as HIPK2 and p300 from proteasome-dependent degradation. We demonstrated that PML inhibits the degradation of HIPK2 and p300 by the ubiquitin-proteasome pathway (Fig. 5A and B) and that this inhibition occurs in NBs (Fig. 5E). PML has been suggested to increase protein stability. For instance, PML enhances p53 stability by sequestering MDM2 in the nucleolus (4) and inhibits p73 ubiquitin-dependent degradation (5, 45). These reports are in agreement with our data showing that PML increases protein stability. In particular, the colocalization of PML in NBs is required for the stabilization of HIPK2, p300, and p73. In contrast, other groups have shown that NBs act as sites for proteasomal protein degradation by recruiting subunits of proteasomes and ubiquitin (2, 34, 35). However, these studies showed only that the ubiquitin-proteasome pathway-related proteins were recruited to NBs. There has been no report showing that proteasomal protein degradation actually occurs in NBs. Therefore, we suggest that PML may regulate protein stability by inhibiting protein degradation within NBs, while still allowing protein degradation by the ubiquitin-proteasome pathway to occur around the outside of NBs. In fact, the components of SCF^{Fbx3} which are essential for the degradation of HIPK2 and p300 were localized at the peripheries of NBs (Fig. 1C). In this way, it would be possible to finely regulate protein stability/degradation at the peripheries of NBs. Thus, it is not surprising in this respect that the proteins linked to degradation, proteasome subunits, and ubiquitin are found in NBs. As for the site of proteasomal protein degradation, Mattsson and coworkers showed that NB-associated proteins move to the nucleolus in the presence of MG132 and that the nucleolus may regulate proteasomal protein degradation (40). In the present study, we detected HIPK2 and p300 outside of NBs in the presence of MG132 but failed to detect PML, HIPK2, or p300 in the nucleolus (Fig. 5E). Although further studies concerning the actual site of proteasomal protein degradation will be required, it is clear from the work presented here and elsewhere that PML is crucial for the ubiquitin-proteasome pathway.

As shown in Fig. 3A, Fbx3 and PML cooperatively activated p53-dependent transcription, and Fbx3 was required for the enhanced transcription activity of p53 mediated by PML (Fig. 3B and C). Furthermore, Fbx3 and PML synergistically enhanced the HIPK2-stimulated transcriptional activity of p53 (Fig. 6B). Since PML stabilized HIPK2 ubiquitinated by Fbx3 (Fig. 6A), these results suggest that the ubiquitination of HIPK2 stimulates the transcriptional activity of p53. Important roles for ubiquitin in transcriptional regulation have been reported (10). The F-box protein Skp2 induces the ubiquitination and degradation of c-Myc but upregulates c-Myc transcriptional activity (29, 55). Likewise, the E3 ubiquitin ligases RSP5 and E6-AP activate hormone receptor-dependent transcription (25, 43), and SCF^{Met30}-induced ubiquitination of VP16 appears to be essential for transcriptional activation (51). Taken together, these findings indicate that stabilizing ubiquitinated HIPK2 appears to upregulate the transcriptional activity of p53 as shown in Fig. 6B. We speculate that ubiquitinated HIPK2 could activate p53-dependent transcription by increasing the phosphorylation of p300 and p53. It is also possible that ubiquitinated HIPK2 and p300 are degraded rapidly after the completion of the transcription of their target genes to ensure the complete shutdown of transcription. The regulation of the exact timing and levels of transcription in this way could constitute a novel mechanism for regulating gene expression.

Dysfunction of HIPK2 and p300 in leukemia pathogenesis. It has been reported that the PML-RARα fusion, which is generated by the chromosome translocation t(15;17) found for APL, forms stable oligomers with normal PML and inhibits PML-mediated transcriptional activation in a dominant-negative manner. We have shown here that PML and PML-RARα play opposite roles in HIPK2 stability (Fig. 7A to D). This may be because PML-RARα disrupts NBs, in which HIPK2 is stabilized as shown in Fig. 5A and E. The result showing that removal of the Fbx3-interacting region of PML-RARα destabilized HIPK2 (see Fig. S4 in the supplemental material) also suggests that the disruption of NBs by PML-RARα decreases protein stability. As PML-RARα enhanced HIPK2 degradation, PML-RARα would repress transcription by destabilizing coactivators such as HIPK2 and p300, perhaps contributing in this way to the pathogenesis of leukemia. Mutations in HIPK2 and p300 have been found for acute myeloid leukemia (AML) and myelodysplastic syndrome. p300 is involved in chromosome translocations such as t(8;22) and t(11;22) found in AML (8, 23, 31). We have recently found mutations in the *HIPK2* gene in association with AML and myelodysplastic syndrome that impair p53- and AML1-mediated transcription (37). These results suggest that dysfunctions of HIPK2 and p300 may be implicated in leukemia.

In summary, we propose that transcription is regulated by SCF^{Fbx3} and PML, as shown in Fig. 7F. According to this model, PML would activate transcription by counteracting the degradation of the transcription coactivators HIPK2 and p300, whose degradation by the ubiquitin-proteasome pathway is mediated by the novel SCF^{Fbx3} ubiquitin ligase. Conversely, PML-RARα would inactivate transcription by blocking the function of PML, thereby enhancing the SCF^{Fbx3}-induced degradation of HIPK2.

ACKNOWLEDGMENTS

We thank Y. Taya (National Cancer Center Research Institute) for kindly providing the cDNAs for p53 cDNA and the MDM2-luc reporter. We also thank Yukiko Aikawa, Noriko Aikawa, and Chikako Hatanaka for technical assistance.

This work was supported in part by grants-in-aid for scientific research from the Ministry of Health, Labor and Welfare and from the Ministry of Education, Culture, Sports, Science and Technology and by the Program for Promotion of Fundamental Studies from the National Institute of Biomedical Innovation of Japan.

REFERENCES

1. Aikawa, Y., L. A. Nguyen, K. Isono, N. Takakura, Y. Tagata, M. L. Schmitz, H. Koseki, and I. Kitabayashi. 2006. Roles of HIPK1 and HIPK2 in AML1- and p300-dependent transcription, hematopoiesis and blood vessel formation. EMBO J. 25:3955–3965.

2. **Anton, L. C., U. Schubert, I. Bacik, M. F. Princiotta, P. A. Wearsch, J. Gibbs, P. M. Day, C. Realini, M. C. Rechsteiner, J. R. Bennink, and J. W. Yewdell.** 1999. Intracellular localization of proteasomal degradation of a viral antigen. J. Cell Biol. 146:113–124.
3. **Avantaggiati, M. L., V. Ogryzko, K. Gardner, A. Giordano, A. S. Levine, and K. Kelly.** 1997. Recruitment of p300/CBP in p53-dependent signal pathways. Cell 89:1175–1184.
4. **Bernardi, R., P. P. Scaglioni, S. Bergmann, H. F. Horn, K. H. Vousden, and P. P. Pandolfi.** 2004. PML regulates p53 stability by sequestering Mdm2 to the nucleolus. Nat. Cell Biol. 6:665–672.
5. **Bernassola, F., P. Salomoni, A. Oberst, C. J. Di Como, M. Pagano, G. Melino, and P. P. Pandolfi.** 2004. Ubiquitin-dependent degradation of p73 is inhibited by PML. J. Exp. Med. 199:1545–1557.
6. **Brouillard, F., and C. E. Cremisi.** 2003. Concomitant increase of histone acetyltransferase activity and degradation of p300 during retinoic acid-induced differentiation of F9 cells. J. Biol. Chem. 278:39509–39516.
7. **Cenciarelli, C., D. S. Chiaur, D. Guardavaccaro, W. Parks, M. Vidal, and M. Pagano.** 1999. Identification of a family of human F-box proteins. Curr. Biol. 9:1177–1179.
8. **Chaffanet, M., L. Gressin, C. Preudhomme, V. Soenen-Cornu, D. Birnbaum, and M. J. Pebusque.** 2000. MOZ is fused to p300 in an acute monocytic leukemia with t(8;22). Genes Chromosomes Cancer 28:138–144.
9. **Chen, J., J. R. St-Germain, and Q. Li.** 2005. B56 regulatory subunit of protein phosphatase 2A mediates valproic acid-induced p300 degradation. Mol. Cell. Biol. 25:525–532.
10. **Conaway, R. C., C. S. Brower, and J. W. Conaway.** 2002. Emerging roles of ubiquitin in transcription regulation. Science 296:1254–1258.
11. **de The, H., C. Chomienne, M. Lanotte, L. Degos, and A. Dejean.** 1990. The t(15;17) translocation of acute promyelocytic leukaemia fuses the retinoic acid receptor alpha gene to a novel transcribed locus. Nature 347:558–561.
12. **de The, H., C. Lavau, A. Marchio, C. Chomienne, L. Degos, and A. Dejean.** 1991. The PML-RAR alpha fusion mRNA generated by the t(15;17) translocation in acute promyelocytic leukemia encodes a functionally altered RAR. Cell 66:675–684.
13. **D'Orazi, G., B. Cecchinelli, T. Bruno, I. Manni, Y. Higashimoto, S. Saito, M. Gostissa, S. Coen, A. Marchetti, G. Del Sal, G. Piaggio, M. Fanciulli, E. Appella, and S. Soddu.** 2002. Homeodomain-interacting protein kinase-2 phosphorylates p53 at Ser 46 and mediates apoptosis. Nat. Cell Biol. 4:11–19.
14. **Dyck, J. A., G. G. Maul, W. H. Miller, Jr., J. D. Chen, A. Kakizuka, and R. M. Evans.** 1994. A novel macromolecular structure is a target of the promyelocyte-retinoic acid receptor oncoprotein. Cell 76:333–343.
15. **Fogal, V., M. Gostissa, P. Sandy, P. Zacchi, T. Sternsdorf, K. Jensen, P. P. Pandolfi, H. Will, C. Schneider, and G. Del Sal.** 2000. Regulation of p53 activity in nuclear bodies by a specific PML isoform. EMBO J. 19:6185–6195.
16. **Gilliland, D. G.** 1998. Molecular genetics of human leukemia. Leukemia 12(Suppl. 1):S7–S12.
17. **Glickman, M. H., and A. Ciechanover.** 2002. The ubiquitin-proteasome proteolytic pathway: destruction for the sake of construction. Physiol. Rev. 82:373–428.
18. **Goddard, A. D., J. Borrow, P. S. Freemont, and E. Solomon.** 1991. Characterization of a zinc finger gene disrupted by the t(15;17) in acute promyelocytic leukemia. Science 254:1371–1374.
19. **Gresko, E., A. Moller, A. Roscic, and M. L. Schmitz.** 2005. Covalent modification of human homeodomain interacting protein kinase 2 by SUMO-1 at lysine 25 affects its stability. Biochem. Biophys. Res. Commun. 329:1293–1299.
20. **Guo, A., P. Salomoni, J. Luo, A. Shih, S. Zhong, W. Gu, and P. P. Pandolfi.** 2000. The function of PML in p53-dependent apoptosis. Nat. Cell Biol. 2:730–736.
21. **Haupt, Y., R. Maya, A. Kazaz, and M. Oren.** 1997. Mdm2 promotes the rapid degradation of p53. Nature 387:296–299.
22. **Hofmann, T. G., A. Moller, H. Sirma, H. Zentgraf, Y. Taya, W. Droge, H. Will, and M. L. Schmitz.** 2002. Regulation of p53 activity by its interaction with homeodomain-interacting protein kinase-2. Nat. Cell Biol. 4:1–10.
23. **Ida, K., I. Kitabayashi, T. Taki, M. Taniwaki, K. Noro, M. Yamamoto, M. Ohki, and Y. Hayashi.** 1997. Adenoviral E1A-associated protein p300 is involved in acute myeloid leukemia with t(11;22)(q23;q13). Blood 90:4699–4704.
24. **Ilyin, G. P., M. Rialland, C. Pigeon, and C. Guguen-Guillouzo.** 2000. cDNA cloning and expression analysis of new members of the mammalian F-box protein family. Genomics 67:40–47.
25. **Imhof, M. O., and D. P. McDonnell.** 1996. Yeast RSP5 and its human homolog hRPF1 potentiate hormone-dependent activation of transcription by human progesterone and glucocorticoid receptors. Mol. Cell. Biol. 16:2594–2605.
26. **Isono, K., K. Nemoto, Y. Li, Y. Takada, R. Suzuki, M. Katsuki, A. Nakagawara, and H. Koseki.** 2006. Overlapping roles for homeodomain-interacting protein kinases Hipk1 and Hipk2 in the mediation of cell growth in response to morphogenetic and genotoxic signals. Mol. Cell. Biol. 26:2758–2771.
27. **Jensen, K., C. Shiels, and P. S. Freemont.** 2001. PML protein isoforms and the RBCC/TRIM motif. Oncogene 20:7223–7233.
28. **Kakizuka, A., W. H. Miller, Jr., K. Umesono, R. P. Warrell, Jr., S. R. Frankel, V. V. Murty, E. Dmitrovsky, and R. M. Evans.** 1991. Chromosomal translocation t(15;17) in human acute promyelocytic leukemia fuses RAR alpha with a novel putative transcription factor, PML. Cell 66:663–674.
29. **Kim, S. Y., A. Herbst, K. A. Tworkowski, S. E. Salghetti, and W. P. Tansey.** 2003. Skp2 regulates Myc protein stability and activity. Mol. Cell 11:1177–1188.
30. **Kipreos, E. T., and M. Pagano.** 2000. The F-box protein family. Genome Biol. 1:REVIEWS3002.
31. **Kitabayashi, I., Y. Aikawa, A. Yokoyama, F. Hosoda, M. Nagai, N. Kakazu, T. Abe, and M. Ohki.** 2001. Fusion of MOZ and p300 histone acetyltransferases in acute monocytic leukemia with a t(8;22)(p11;q13) chromosome translocation. Leukemia 15:89–94.
32. **Kitabayashi, I., A. Yokoyama, K. Shimizu, and M. Ohki.** 1998. Interaction and functional cooperation of the leukemia-associated factors AML1 and p300 in myeloid cell differentiation. EMBO J. 17:2994–3004.
33. **Kubbutat, M. H., S. N. Jones, and K. H. Vousden.** 1997. Regulation of p53 stability by Mdm2. Nature 387:299–303.
34. **Lafarga, M., M. T. Berciano, E. Pena, I. Mayo, J. G. Castano, D. Bohmann, J. P. Rodrigues, J. P. Tavanez, and M. Carmo-Fonseca.** 2002. Clastosome: a subtype of nuclear body enriched in 19S and 20S proteasomes, ubiquitin, and protein substrates of proteasome. Mol. Biol. Cell 13:2771–2782.
35. **Lallemand-Breitenbach, V., J. Zhu, F. Puvion, M. Koken, N. Honore, A. Doubeikovsky, E. Duprez, P. P. Pandolfi, E. Puvion, P. Freemont, and H. de The.** 2001. Role of promyelocytic leukemia (PML) sumolation in nuclear body formation, 11S proteasome recruitment, and As2O3-induced PML or PML/retinoic acid receptor alpha degradation. J. Exp. Med. 193:1361–1371.
36. **Li, Q., A. Su, J. Chen, Y. A. Lefebvre, and R. J. Hache.** 2002. Attenuation of glucocorticoid signaling through targeted degradation of p300 via the 26S proteasome pathway. Mol. Endocrinol. 16:2819–2827.
37. **Li, X. L., Y. Arai, H. Harada, Y. Shima, H. Yoshida, S. Rokudai, Y. Aikawa, A. Kimura, and I. Kitabayashi.** 2007. Mutations of the HIPK2 gene in acute myeloid leukemia and myelodysplastic syndrome impair AML1- and p53-mediated transcription. Oncogene 26:7231–7239.
38. **Lill, N. L., S. R. Grossman, D. Ginsberg, J. DeCaprio, and D. M. Livingston.** 1997. Binding and modulation of p53 by p300/CBP coactivators. Nature 387:823–827.
39. **Look, A. T.** 1997. Oncogenic transcription factors in the human acute leukemias. Science 278:1059–1064.
40. **Mattsson, K., K. Pokrovskaja, C. Kiss, G. Klein, and L. Szekely.** 2001. Proteins associated with the promyelocytic leukemia gene product (PML)-containing nuclear body move to the nucleolus upon inhibition of proteasome-dependent protein degradation. Proc. Natl. Acad. Sci. USA 98:1012–1017.
41. **Miyoshi, H., K. Shimizu, T. Kozu, N. Maseki, Y. Kaneko, and M. Ohki.** 1991. t(8;21) breakpoints on chromosome 21 in acute myeloid leukemia are clustered within a limited region of a single gene, AML1. Proc. Natl. Acad. Sci. USA 88:10431–10434.
42. **Moller, A., H. Sirma, T. G. Hofmann, S. Rueffer, E. Klimczak, W. Droge, H. Will, and M. L. Schmitz.** 2003. PML is required for homeodomain-interacting protein kinase 2 (HIPK2)-mediated p53 phosphorylation and cell cycle arrest but is dispensable for the formation of HIPK domains. Cancer Res. 63:4310–4314.
43. **Nawaz, Z., D. M. Lonard, C. L. Smith, E. Lev-Lehman, S. Y. Tsai, M. J. Tsai, and B. W. O'Malley.** 1999. The Angelman syndrome-associated protein, E6-AP, is a coactivator for the nuclear hormone receptor superfamily. Mol. Cell. Biol. 19:1182–1189.
44. **Nguyen, L. A., P. P. Pandolfi, Y. Aikawa, Y. Tagata, M. Ohki, and I. Kitabayashi.** 2005. Physical and functional link of the leukemia-associated factors AML1 and PML. Blood 105:292–300.
45. **Oberst, A., M. Rossi, P. Salomoni, P. P. Pandolfi, M. Oren, G. Melino, and F. Bernassola.** 2005. Regulation of the p73 protein stability and degradation. Biochem. Biophys. Res. Commun. 331:707–712.
46. **Pearson, M., R. Carbone, C. Sebastiani, M. Cioce, M. Fagioli, S. Saito, Y. Higashimoto, E. Appella, S. Minucci, P. P. Pandolfi, and P. G. Pelicci.** 2000. PML regulates p53 acetylation and premature senescence induced by oncogenic Ras. Nature 406:207–210.
47. **Poizat, C., P. L. Puri, Y. Bai, and L. Kedes.** 2005. Phosphorylation-dependent degradation of p300 by doxorubicin-activated p38 mitogen-activated protein kinase in cardiac cells. Mol. Cell. Biol. 25:2673–2687.
48. **Poizat, C., V. Sartorelli, G. Chung, R. A. Kloner, and L. Kedes.** 2000. Proteasome-mediated degradation of the coactivator p300 impairs cardiac transcription. Mol. Cell. Biol. 20:8643–8654.
49. **Rabbitts, T. H.** 1994. Chromosomal translocations in human cancer. Nature 372:143–149.
50. **Rinaldo, C., A. Prodosmo, F. Mancini, S. Iacovelli, A. Sacchi, F. Moretti, and S. Soddu.** 2007. MDM2-regulated degradation of HIPK2 prevents p53Ser46 phosphorylation and DNA damage-induced apoptosis. Mol. Cell 25:739–750.
51. **Salghetti, S. E., A. A. Caudy, J. G. Chenoweth, and W. P. Tansey.** 2001.